

Modeling Nutrient-Enriched Sediments Transport During Coastal Erosion Processes

**Final Project Report
(January 1999 – March 2001)**

Submitted to

Ohio Lake Erie Protection Fund (LEPF)

By

**Principal Investigator: Dr. Ron Li
Researchers: T. Ali, R. Ma and Dr. K. Di**

**Department of Civil and Environmental Engineering
and Geodetic Science
The Ohio State University**

March 2001

Table of Contents

1. Introduction	1
1.1 Background	1
1.2 Study area.....	2
1.3 Research group at OSU	3
1.4 Project products	4
2. Data Description and Preparation	7
2.1 NOAA Aerial photographs.....	8
2.2 Hypsographic and hydrographic Digital Line Graphs (DLGs)	8
2.3 Soil data	9
2.4 Digital Elevation Models (DEMs)	11
2.5 USGS Stream Discharge Data.....	12
2.6 Precipitation Data	13
2.7 Land-use Data.....	14
2.8 USGS Daily Suspended-Sediment Data.....	14
2.9 Phosphorus Data.....	14
2.10 The Lake Erie Bathymetry	15
3. Shoreline Extraction from Multiple Data Sources	16
3.1 Shoreline digitized from aerial orthophotos	17
3.2 3D shoreline extracted from simulated IKONOS imagery	18
3.3 Digital shoreline through the intersection between CTM and water surface	20
3.4 CTM generation	21
3.5 A Method for digital shoreline extraction	22
3.6 Accuracy analysis	25
3.7 Shoreline prediction using linear regression and EPR	30
4. Modeling shoreline erosion and coastal transported sediment	38
4.1 GPS field surveying	39

1. Introduction

1.1 Background

It is well known that the spatial characteristics of the terrain strongly affect surface flow and sediment transport processes. Soil erosion is a major source of the sediment that is transported with surface flow or washed by coastal waves and currents. Furthermore, surface flow washes excess chemical fertilizers from croplands, causing non-point-source pollution. This study is focused on modeling contaminated sediment transport during coastal erosion processes, treating shoreline erosion as a source for the coastal sediment. Up to now, there have been elaborate flow models and pollutant transport models in use at the watershed scale. Yet, these models focus mainly on the detailed description of small-scale physical phenomena.

Many researchers have considered a GIS coupled with environmental and hydrologic models to be suitable for this purpose and have adopted this technology in a wide range of studies. It is clear that the use of GIS places some constraints on the representational scope of the coupled system, since GIS are layer based geometry-indexed systems. The importance of this study comes from the fact that relatively little research work has been done on performing *large scale* modeling for such applications using the methods investigated here.

It is commonly known that agricultural activity endangers the quality of nearby surface waters. Farmers may apply chemical nutrients to increase soil fertility and use pesticides to control unwanted plants and destructive insects. Numerous studies have been performed at a small scale to estimate soil erosion and nutrient-enriched sediment transport from croplands. But until recently few studies have been conducted to evaluate the contamination of water bodies, such as Lake Erie, from the nutrient-enriched sediment transported by surface flow from croplands during erosion processes. The environmental, economic, and aesthetic impacts caused by these processes could make them a formidable regional problem.

So as to study the processes that transport nutrient-enriched sediment in the coastal environment in an efficient way, a conceptual framework needs to be established. These processes are either water-based, that is, resulting in direct coastal sediment load, or land-based, that is, driven by the surface runoff resulting from precipitation and snowmelt. The water-based processes are driven mainly by the mechanism of the waves and currents in the near-shore zone. This later process is responsible for shoreline erosion that is directly related to the coastal sedimentation phenomenon. The land-based sediment transport process is responsible for the terrain surface change due to the wear of the top-most soil layer. In this research, these two processes have been investigated in-depth for the study area, at a large-scale, using the datasets that are described in the following section.

1.2 Study area

The project site has been selected in a Lake Erie coastal area that extends for eleven-km from Sheldon Marsh Preserve to Vermillion along the southern shore of Lake Erie from longitude 82°40'37 " W to 82°28'24" W. Figure 1.1 shows the research area of the project. Part of this area is farmland, where heavy phosphorus-based fertilizers are applied to the soil, and as well, severe erosion has been taking place along the shoreline.

The land use and farming information and total phosphorus distribution have been managed in the GIS environment. New, innovative, GIS-based models that quantitatively represent sediment transport processes in the study area during erosion processes have been developed.

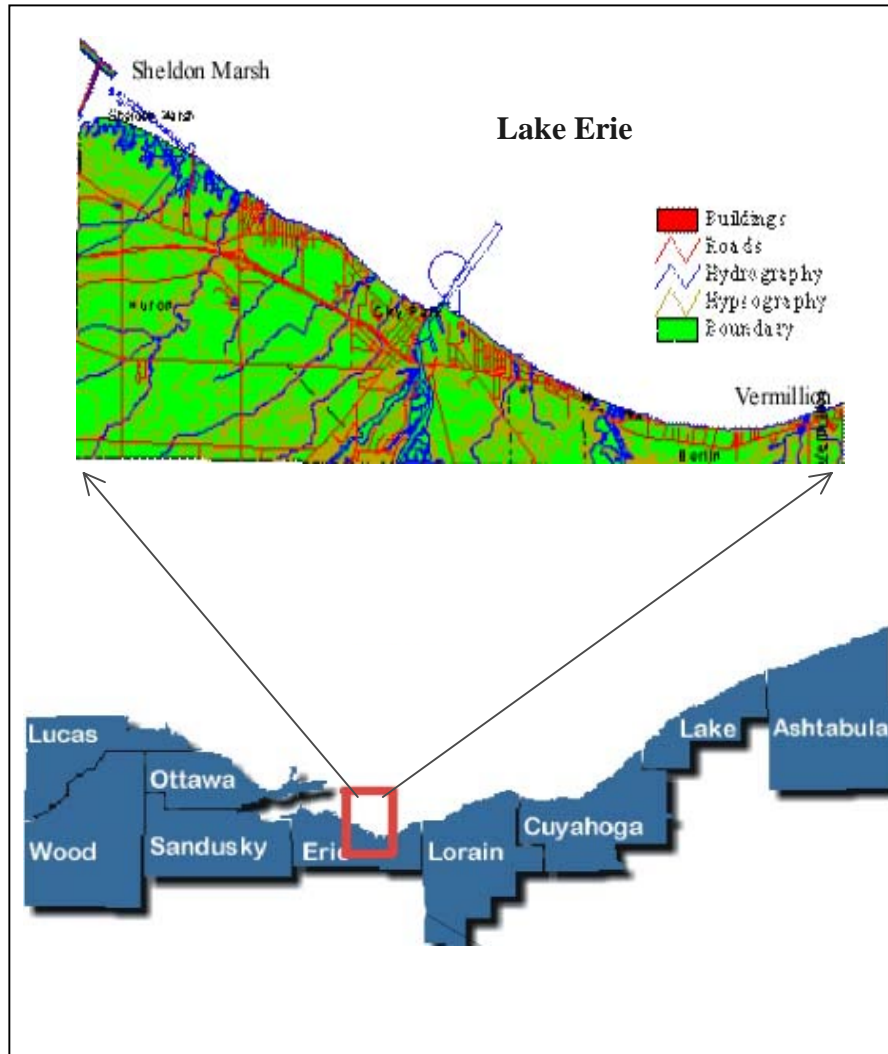


Figure 1.1. The study area

1.3 Research Group at OSU

The research group at the Ohio State University consists of:

Principal investigator: Dr. Ron Li

Post-doctoral fellow: Dr. K. Di

Graduate Assistants: T. Ali and R. Ma

1.4 Project products

The products and the findings of this project include analytical models, scientific papers, spatial databases, and a software system. Some of these products are listed below:

1.4.1 Publications

- Li, R., J.-K. Liu and Y. Felus 1999, Spatial Modeling and Analysis for Shoreline Change Detection and Coastal Erosion Monitoring, Geoinformatics 1999, Ann Arbor, MI, June 19-21 1999.
- Li, R. and G. Zhou 1999, Experimental Study on Ground Point Determination from High Resolution Airborne and Satellite Imagery, ASPRS Annual Conference, Portland, OR, May 17-21 1999.
- Tarig Ali, 1999, GIS Modeling of Phosphorus Concentration, Soil Loss due to Water Erosion and Coastal Terrain Change Detection in Lake Erie Coastal Areas, MS. Thesis, The Ohio State University.
- Ali, T. and R. Li 2000, Spatial-temporal Modeling of Soil Erosion and Contaminated Sediment Transport in Lake Erie Coastal Area, ASPRS Annual Conference, Washington, D.C., May 22-26 2000.
- Zhou, G., and R. Li 2000, Accuracy Evaluation of Ground Points from IKONOS High-Resolution Satellite Imagery. Photogrammetric Engineering and Remote Sensing, 66(9): 1103-1112.
- Ali, T., R. Ma and R. Li 2001, Assessment of the Variability of Phosphorus Intensity and Sediment Supply Profiles with Topography in a Lake Erie Coastal Area, the 4th International Symposium on Computer Mapping and GIS for Coastal Zone Management, Halifax, Nova Scotia, Canada, June 18- 20, 2001, accepted.
- Li, R., G. Zhou, N.J. Schmidt, C. Fowler and G. Tuell 2001, Photogrammetric Processing of High-Resolution Airborne and Satellite Linear Array Stereo Images for Mapping Applications. International Journal of Remote Sensing, Accepted.

- Di, K., R. Ma and R. Li, 2001, Deriving 3-D shorelines from high-resolution IKONOS satellite images with rational functions, ASPRS Annual Conference, St. Louis, April 23-27 2001.

1.4.2 Databases

- Sedimentation-Erosion database,
- RUSLE model results database,
- Phosphorus land use soil-types data set,
- GPS control points of 2000 in the Lake Erie research area,
- Aerial photos for 1997 in the Lake Erie research area acquired by NOAA,
- IKONOS simulated imagery for 1997, and
- IKONOS 4m multispectral satellite images for 2001.

1.4.3 Shorelines

- Shoreline derived from aerial photos acquired by NOAA in 1997,
- Digital shoreline derived from the intersection between the CTM and the water level of 1997,
- Shoreline computed from simulated IKONOS images for 1997,
- Shoreline derived from a USGS 1:24,000 DLG for 1979,
- Shoreline provided by ODNR for 1973,
- Shoreline provided by ODNR for 1990, and
- Shoreline digitized from NOAA t-sheet for 1973.

1.4.4 Software and Models

- Models developed in a GIS to perform environmental analysis (Runoff Model, Sedimentation-Erosion Model, and Runoff-phosphorus Model),
- Bundle adjustment software for processing one-meter resolution satellite imagery (mainly supported by a NOAA project),
- Software for simulating high resolution satellite imagery based on raw aerial photos and ortho images (mainly supported by a NOAA project), and

- A model developed in ERDAS to extract a digital shoreline from the intersection between a CTM and a water level.

2. Data Description and Preparation

This study uses both raster and vector data sets from different sources, to model spatially and temporally the crucial processes of soil erosion and contaminated sediment transport in the study area. Raster data sets have values stored in a uniform rectangular array and are typically referred to as grids or digital elevation models. Vector data sets include points, lines and polygons and are typically referred to as coverages. Vector data sets also have tables associated with them that describe features they represent (ESRI, 1991). The Arc/Info GIS system supports transformations between the raster and vector data sets. A standard map projection is needed for any research study where spatial analysis of geographic data from different sources is required. The spatial data sets are available at various map scales and in different coordinate systems.

Arc/Info GIS allows for the successful adjoining of spatial data, even if the data are of different spatial scales, as long as those data have a common datum and map projection, and it also allows the user to convert data from one specific map projection to another. Using the *projectdefine* and *project* Arc/Info commands that are available at the Arc prompt (where necessary), the following projection parameters (Table 2.1) are defined for every layer used in this study. The establishment of a digital database for the study area involves the assembly of the data that are used for each of the subsequent stages of this study. This section describes the different data sets and discusses how they will be managed for their ultimate use by this research.

Table 2.1 The study-area projection parameters

Map projection	UTM
Zone	17
Datum	NAD27
Spheroid	CLARKE1866
Units	METERS

2.1 NOAA aerial photographs

This is a set of NOAA-NGS aerial photographs that were acquired in mid July 1997. The data have been used to produce a 2.5-meters Digital Elevation Model (DEM), a Coastal Terrain Model (CTM), and a corresponding set of orthophotos (rectified aerial photographs). The resulting set of orthophotos has been used to extract the 1997-shoreline and further used to estimate the shoreline erosion in the period 1979-1997. There are a total of 12 color photos at the scale of 1/20,000. The pixel size is about a half meter. The camera is a Wild RC30* and the lens is a Wild Universal Aviogon A4-F. More description about the camera can be found in the Report of Calibration of Aerial Mapping Camera from the United States Department of the Interior. These photos cover the research area from Sheldon Marsh in the west to the Old Women Creek.

2.2 Hypsographic and Hydrographic Digital Line Graphs (DLGs)

Digital line graph (DLG) data are digital representations of cartographic information. The 1:24,000-scale Hypsographic and Hydrographic Digital Line Graph (DLG) data files are derived from USGS topographic quadrangle maps. The contour interval of the hypsographic layer is 5 feet. The 1:24,000 digital line graphs are available in either standard or optional formats. The standard format has a larger logical record length (144 bytes) than the optional format (80 bytes), but is projected in an internal file coordinate system (thousandths of a map inch) that is not as easy to work with as the Universal Transverse Mercator (UTM) projection of the optional. Therefore, the optional format has been chosen for the study. All DLG data distributed by the USGS are DLG – Level 3 (DLG-3), which means that the data contain a full range of attribute codes, have full topological structuring, and have passed certain quality-control checks. This is a data-set level implementation of the Federal Geographic Data Committee's Content Standards for Digital Geospatial Metadata format. These data sets are available publicly through the Internet. Before manipulation of these files could be performed, they had to be converted into the Arc/Info GIS system format. The *dlgarc* command, with the optional format argument specified, is used for this purpose. Once the vector data are imported into Arc/Info, their topology is built using the *build* command, which creates and/or updates feature attribute tables for an Arc/Info coverage (Figure 2.1).

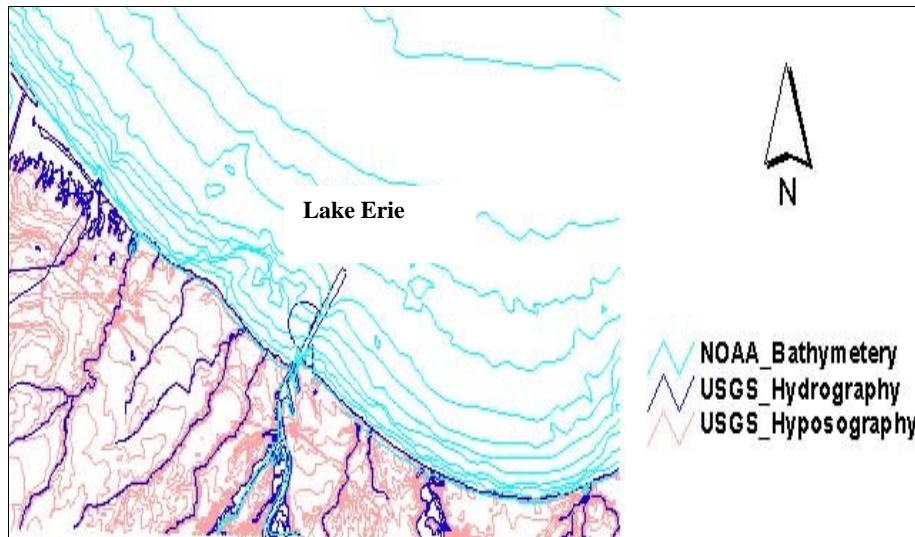


Figure 2.1. The USGS Hypsographic and Hydrographic layers

2.3 Soil Data

The soil data set is one of the primary data sets used in this study, for the reason that it determines soil erosion characteristics and affects the estimation of the RUSLE model parameters. The soil data set for this study was obtained from the office of the Erie Soil and Water Conservation District, Erie County Service Center located in Sandusky Ohio. The data are a result of a soil survey for which the major fieldwork was done in the period 1963-1965. Soil names and descriptions were approved in 1969. The soil map was digitized from the survey book of Erie County, Ohio (Erie County Soil Survey Book, 1971), then edited and added to the study database after projecting the resultant soil coverage to the chosen map projection described earlier (see Figure 2.2). The characteristics of the major soil associations in the area for the study area are shown below (Erie County Soil Survey Book, 1971):

2.3.1 Kibbie-Tuscola-Colwood association

It are deep, level to gently sloping, moderately well drained to very poorly drained soils that have a silt loam to silty clay loam subsoil, on old lakebeds. Kibbie soil was chosen to represent this category for this study. These soils were formed in limy silt and

fine sand deposited when the level of Lake Erie was higher. This association makes up about 15 percent of the county. It is about 35 percent Kibbie soils, 35 percent Tuscola soils, 20 percent Colwood soils, and the rest minor soils. Kibbie soils are nearly level, somewhat poorly drained, and light colored. Tuscola soils are nearly level to gently sloping and moderately well drained. Colwood soils are level to depressional, very poorly drained, and dark colored. Nearly all of this association is cropland. The principal crops are corn, soybeans, and wheat. These soils are productive, and the crops respond well to fertilization, but seasonal wetness is the main limitation.

2.3.2 Del Rey-Lenawee association

It is deep, nearly level, somewhat poorly drained to very poorly drained soils that have subsoil of silty clay to silty clay loam, on old lakebeds. Del Rey was chosen to represent this category for this study. This association makes up about 10 percent of the county. It is about 60 percent Del Rey soils, 30 percent Lenawee soils, and 10 percent minor soils. Del Rey soils are somewhat poorly drained and light colored. Lenawee soils are nearly level to depressional, very poorly drained, and dark colored. Nearly all of this association is cropland. The principal general crops are corn, soybeans, and wheat.

2.3.3 Marsh and Beaches association

Level marsh and well drained beaches adjacent to Lake Erie. Beaches was chosen to represent this category for this study. This association occurs as scattered areas adjacent to Lake Erie. It makes up about 6 percent of the county. Marsh is slightly below the level of the lake most of the year. Fluctuations in the level of the lake result in the growth of cattails, willows, and other marsh vegetation. Marsh is suitable for wildlife habitat.

2.3.4 Mohoning-Bogart-Haskins- Jimtown association

It is deep, nearly level to gently sloping, poorly drained to moderately well drained soils that have a subsoil of sandy loam to clay; on uplands, terraces, and beach ridges. Haskins was chosen to represent this category. This association makes up about 19 percent of the county. About 70 percent of this association is cropland. Corn, wheat, oats, and meadow are important crops. Orchard crops, soybeans, and some vegetables are

grown on the beach ridges. If limed, the soils are moderately productive. Lime is needed to get the maximum response from fertilizers. The main limitations are inadequate drainage, seasonal wetness, and low fertility. The map of Figure 2.2 shows the soils distribution of the representative soil types in the study area.

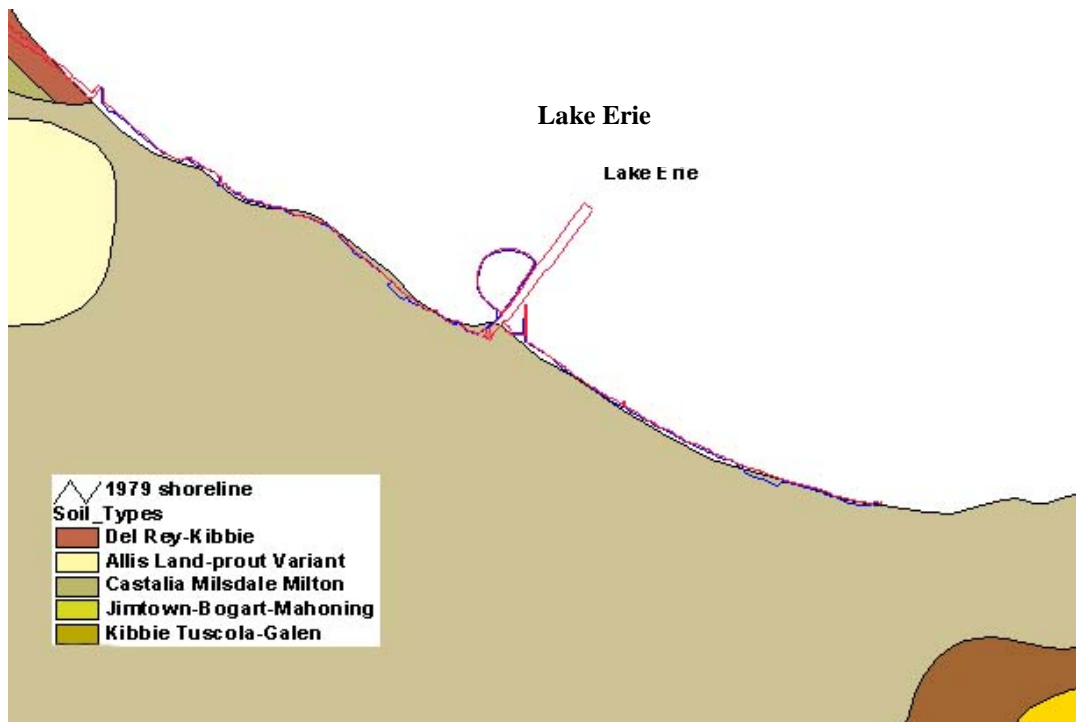


Figure 2.2. A map shows the major soil series in the study area

2.4 Digital Elevation Models (DEMs)

The USGS Digital Elevation Model (DEM) data files are digital representations of cartographic information in a raster form. DEMs consist of a sampled array of elevations for a number of ground positions at regularly spaced intervals. These digital cartographic and geographic data files are produced by the U.S. Geological Survey (USGS) as part of the National Mapping Program and are available in 7.5-minute, 15-minute, 2-arc-second (also known as 30-minute), and 1-degree units. The 7.5- and 15-minute DEMs are included in the large-scale category while 2-arc-second DEMs fall within the intermediate scale category and 1-degree DEMs fall within the small-scale category

(USGS, 1990). The DEM data for 7.5-minute units correspond to the USGS 1:24,000 and 1:25,000 scale topographic quadrangle map series for all of the United States and its territories. Each 7.5-minute DEM is based on 30- by 30-meter data spacing with the Universal Transverse Mercator (UTM) projection. Each 7.5- by 7.5-minute block provides the same coverage as the standard USGS 7.5-minute map series. The vertical accuracy of 7.5-minute DEMs is equal to or better than 15 meters. A minimum of 28 test points per DEM is required (20 interior points and 8 edge points). The accuracy of the 7.5-minute DEM data, together with the data spacing, adequately support computer applications that analyze hypsographic features to a level of detail similar to manual interpretations of information as printed at map scales not larger than 1:24,000 scale. This data set has been used for comparison with the DEM created using the 1:24,000 DLG coverage. The same quality checks performed for the DLG files discussed above have been applied for this set as well.

2.5 USGS Stream Discharge Data

Daily average discharge data are available for all Ohio active streams from the USGS through the Ohio NWIS-W Data Retrieval Web server at the Internet site (<http://waterdata.usgs.gov/nwis-w/OH/>). These discharge values recorded by each USGS gauge represent the average stream-flow at the gauge for a particular day. Daily, monthly, and annual Stream-flow volumes are calculated by processing the raw discharge data. Geographic locations in latitudes and longitudes of the USGS stream flow gauges are available from the same site above. A point coverage of this digital coordinate data is built using the Arc/Info *generate* command, specifying points as the spatial feature type. Once the coverage is created, point topology is established using the *build* command and, using the *addxy* command, the digital coordinate values are added as attributes to each point. The attribute data is then added to the gauge stations point attribute table using the Arc/Info *Joinitem* command. This command links data from two tables through the use of a common relate item. Finally, the stream gauge coverage is converted from geographic to the UTM projection, using ARC Tools. The resulting stream gauge coverage shows the location of the USGS stream gauge within the study area and is used to define the basin

outlet that helps in delineating the study area boundary needed for the hydrologic modeling and analysis.

2.6 Precipitation Data

A rainfall data set is the backbone of any hydrologic study and is a primary input to any research on non-point source pollution modeling or analysis. Collins and Dickey (1989) employed a least-squares optimization procedure to develop a stochastic model for simulating individual rainfall-runoff events and performing non-point source pollutant load assessments. They found that variations in the selected rainfall time step interval can significantly affect estimates of runoff, sediment yield, and erosion characteristics in some non-point source pollution models that accept non-steady state rainfall inputs. This study considered precipitation as a steady state quantity averaged over an extended (30 year) time period. Precipitation data for this study were obtained from the Oregon State University Forestry Sciences Laboratory Web site in Arc/Info interchange format (E00) and were imported as coverages using the *import* command. This data set was developed at the Oregon State University Forestry Sciences Laboratory. These files are part of the Parameter-elevation Regressions on Independent Slopes Model (PRISM), which covers the whole United States. PRISM is an analytical model that uses precipitation data measured at over 7,000 National Weather Service and cooperator stations, 500 SNOTEL stations, and some selected state network stations (Daly et al., 1994). Estimated precipitation values are established for intermediate grid-cells that have been created from these coverages through the use of a regression function, considering the measured precipitation point data along with digital elevation model data to account for topographic effects (modified from Daly et al., 1994). The result of this process is a completely gridded surface of average precipitation across the study area. Average monthly (January through December) and average annual precipitation grids for the period between 1961 and 1990 were then prepared for this study representing a temporal data set of precipitation over monthly time periods.

2.7 Land Use Data

This data set is obtained through manual interpretation of aerial photographs acquired from the National Oceanic and Atmospheric Administration (NOAA). The photographs of this area were taken in early 1997. These photos are brought into Arc/Info as background coverages and then both digitization and interpretation were used to create the land use coverage that is used in this study.

2.8 USGS Daily Suspended-Sediment Data

The U.S. Geological Survey has operated a number of daily-suspended sediment stations throughout the country, paid for through a variety of cooperative and federal programs. Daily records, which are used in this study, are prepared for sites where sufficient determination of sediment concentration and water discharge is obtained to justify computation of daily sediment discharge. This database provides station identification number, date, daily mean stream flow discharge in cubic feet per second, daily mean stream flow discharge in cubic meters per second, daily mean suspended-sediment concentration in milligrams per liter, suspended-sediment discharge in tons per day, and suspended sediment discharge in metric tons per day. Each day's data are written to a separate line in a file and data values are separated by spaces. The data set used in this study is available for the period (1987-1990) from the USGS suspended-sediment database. This data set has been prepared and refined to get the approximate loads of sediment corresponding to the study area.

2.9 Phosphorus Data

In order to calculate loading of pollutants from each grid cell, or TIN patch, in the study area, phosphorus concentrations need to be associated with these spatial objects. Using expected mean concentrations associated with land use is one way to assign

spatially-averaged pollutant concentrations; associating concentrations with soil types is another way. Both of these two methods have been integrated in this research to model phosphorus concentrations. For this study, a set of expected mean phosphorus concentrations resulting from a previous National Estuary Program analysis (Baird et al., 1996) were applied to the land uses in the study area. These expected mean concentrations of phosphorus are shown in Table 2.2. Phosphorus concentrations resulting from the National Estuary Program analysis are adjusted using results of another phosphorus analysis of major soil series in the Lake Erie Basin (Logan, 1989). Table 2.2 shows the adjusted phosphorus concentrations that are used in this study.

Land Use Category	Total Phosphorus Concentration (mg/l)
Urban – Residential	0.57
Urban – Commercial	0.32
Urban – Mixed	0.35
Transportation	0.22
Croplands	1.30
Undeveloped/Rangelands	0.12

Table 2.2 Expected phosphorus concentration used in this study

2.10 The Lake Bathymetry

The original bathymetry data is produced by the National Geographical Data Center, NGDC of NOAA and is available in Arc/Info[®] format. The elevation is referenced to the International Great Lakes Datum of 1955, IGLD55 in which the mean low water datum is 570.5 feet above the mean sea level. This bathymetry data was converted into elevation using the relation $570.5 - Z$, where Z is the depth relative to the water datum.

3. Shoreline Extraction from Multiple Data Sources

To study the potential of the one-meter resolution satellite imagery for coastal error mapping and sediment monitoring, we extracted several shorelines with different methods and using different data sets. The resulted accuracies of the shorelines were found to be different as introduced by the methodology and the data source.

The shorelines used to monitor the changes are so-called tide-coordinated shorelines, which are defined by the intersection of the land and desired water level based on tidal observations accumulated over the last 19.2 lunar years. The implementation can be performed by an intersection between the Coastal Terrain Model (CTM) and the water surface model. The tide-coordinate shorelines used by NGS/NOAA are the MLLW (Mean Lower Low Water) and MHW (Mean High Water) shorelines.

The problem is that it is not easy to get tide-coordinated shoreline directly because the shoreline we usually get is instantaneous shoreline and taken at a time when the water level is not at the MLLW level. To get the tide-coordinated shoreline, we may interpolate the instantaneous shorelines by comparing the water levels with the MLLW level. In this project, we obtained shorelines from orthophoto digitization, from CTM and water level intersection, and from simulated IKONOS imagery computation.

The NGS/NOAA photos we used in this project were tide-coordinated, so the shoreline digitized from the orthophoto is considered to be also tide-coordinated. It is the base shoreline in evaluating other shorelines. We analyzed the accuracy of every shoreline we obtained. The accuracies for the estimated aerial shoreline, digital shoreline and IKONOS shoreline are about 1 meter, 2.23 meters, and 4 meters, respectively. In this chapter, we will discuss the methodology of shoreline generation and their accuracies:

- How to extract a 3-D shoreline from orthophotos and further from simulated IKONOS imagery using Rational Functions (RF) and corresponding accuracy.

- How to produce CTM and how to obtain the digital shoreline by an intersection between the CTM and the water surface.
- Accuracy analysis of each shoreline produced in this study.

3.1 Shoreline digitized from aerial orthophotos

The orthophoto pieces were mosaiced together to form a single image mosaic covering the study area. The shoreline was digitized from the orthophoto by manual interpretation. Figure 3.1 shows the digitized shoreline along with the orthophoto. To digitize the shoreline, the image was zoomed in to 4 times the actual size so that we could obtain an accuracy up to 0.25 pixels which corresponds to 0.25m on the ground. During the digitization, manual interpretation was needed, since trees obscure some parts of the shoreline and some parts are difficult to distinguish. This work was completed in ERDAS Imagine. The accuracy of shoreline mainly depends on the accuracy of the orthophoto and the method of digitization. The standard deviation (SD) of the orthophoto position was about 2.26 meters, about 1.6 meters in X and Y directions.

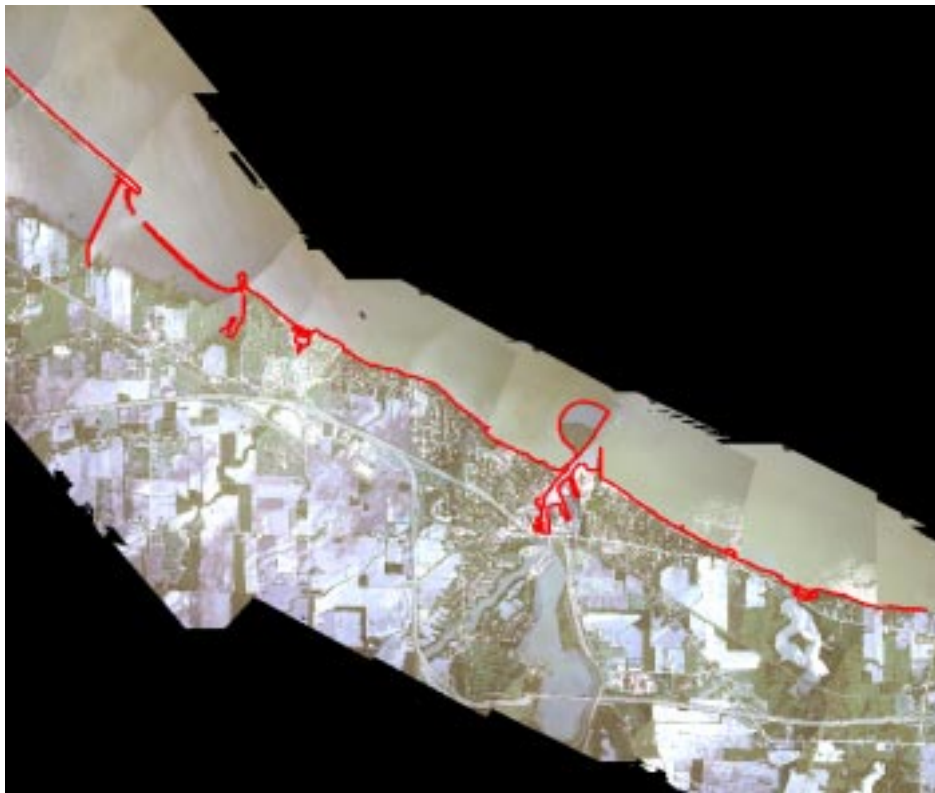


Figure 3.1 Shoreline digitized from the orthophoto

3.2 3D Shoreline extraction from simulated IKONOS imagery

Given stereo IKONOS images and the corresponding upward or downward Rational Function (RF) coefficients, the steps for deriving a 3D shoreline can be summarized as follows.

- Step 1. Manually digitize conjugate shoreline points in both of the stereo images. This step might be accomplished by some automatic recognition and matching techniques in the future.
- Step 2. Normalize the image coordinates of the shoreline points by offsetting and scaling to $[-1, +1]$ with the normalized image coefficients.
- Step 3. Compute the 3D ground positions from these conjugate points iteratively using the method of three-line stereo mapping developed in our NOAA supported project. The ground coordinates now are within the range $[-1, +1]$.
- Step 4. Transform the calculated ground coordinates to unnormalized values.
- Step 5. Repeat Steps 2 to 4 to process the shoreline points one by one, until all points are processed. Thus, the 3D shoreline is constructed.

In this experiment, the 3D data set of the shoreline derived from the aerial orthoimage is the tide-coordinated shoreline and points along it are considered to be the “true” positions. These shoreline points were projected to the simulated fore-, nadir-, and aft-looking IKONOS images using the rigorous sensor model. The corresponding 2D image points were obtained after the projection. This replaced Step 1 and saved a significant amount of time for the experiment. Using the downward and upward RFs coefficients, the 3D-shoreline points were recalculated from the corresponding image points. Fore and aft images were used for space intersection with downward and upward RFs, and all three images were used for upward RFs for comparison. Figure 3.2 shows the computed shoreline from the simulated IKONOS imagery. The 3D-shoreline points were compared with the “true” ones, and the accuracies are summarized in Table 3.1.

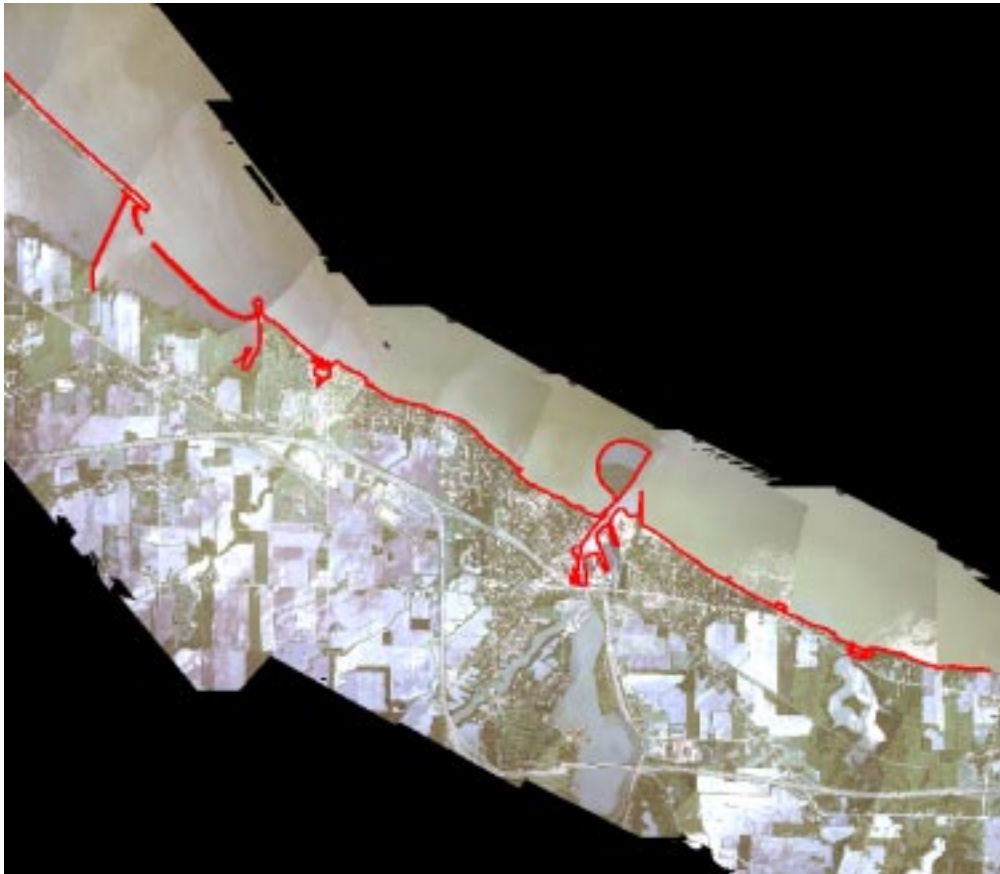


Figure 3.2. Shoreline computed from IKONOS image

We can see from the following table that the intersection with the upward RFs produces more accurate results than the downward RFs; using 3 images with upward RFs gives a slightly better result than using 2 images. Therefore, 3 or more images can be used simultaneously to achieve a high accuracy.

Table 3.1. RMS of shoreline points computed using differences between shorelines derived from the simulated IKONOS images and the tide-coordinated shoreline

	Downward RFs	Upward RFs	
	Fore and aft images	Fore, nadir, and aft images	Fore and aft images
RMS X (m)	1.551817×10^{-6}	6.507232×10^{-11}	8.732452×10^{-11}
RMS Y (m)	1.899339×10^{-7}	1.970419×10^{-11}	4.405990×10^{-11}
RMS Z (m)	2.485093×10^{-6}	6.774642×10^{-11}	8.198980×10^{-11}

The accuracy of the shoreline extracted from the simulated stereo IKONOS images can be approximately estimated based on the error propagation principle. Considering that the accuracy of 3D ground points reaches 2-3m with GCPs (Zhou and Li 2000), and the accuracy of identifying and locating conjugate shoreline points is about 1-2 pixel (1-2m), the accuracy of the shoreline should be below 4m. To get a consistency assessment, the differences between the tide-coordinated shoreline from the orthophoto (“true” shoreline) and the shoreline from the simulated IKONOS imagery listed in Table 3.1 represent the relative accuracy.

3.3 Digital shoreline through the intersection between the CTM and water surface

The land is represented by a CTM and the water surface by the water level. We can determine the instantaneous shoreline by intersecting the CTM and the water level. In nature, the CTM and water level are always changing over time. The CTM changes due to erosion, land use changes, and/or human activities. But in a short period, the CTM change is not significant. So, if we can assume that the CTM is static during a short period, then we can assume that the water level is the only cause of instantaneous shoreline change. The shorelines we measure from non tide-coordinated images are generally instantaneous shorelines. The water level data is from the GLFS (Great Lakes Forecast System).

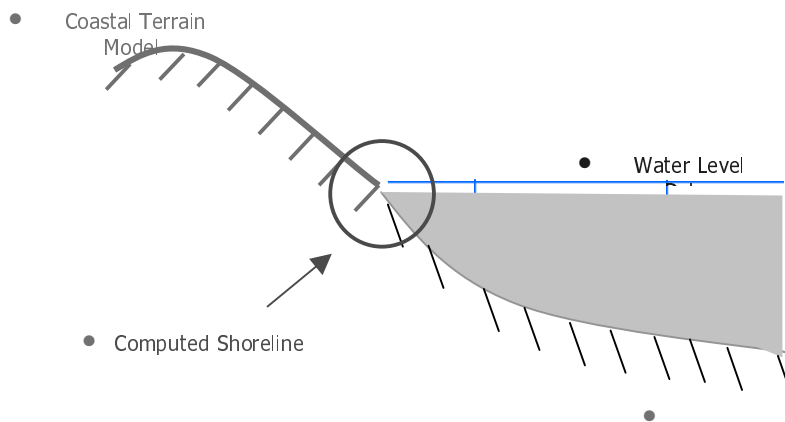


Figure 3.3. Intersection between the CTM and

The GLFS is an operational system developed by the Ohio State University (OSU) and the National Oceanic and Atmospheric Administration (NOAA) Great Lakes Environmental Research Laboratory (GLERL). This System makes regularly scheduled predictions of the physical and other related variables of the Great Lakes. The core calculations are made with a 3D, primitive equation, time dependent, sigma coordinate, free surface, coastal ocean circulation model.

3.4 CTM generation

CTM (Coastal Terrain Model) is defined as the digital surface model of the strip along the shoreline with onshore elevation and near shore bathymetry. It combines the terrain of the land area and the sea area. To obtain the CTM, we need to integrate the terrain models of the land and water areas. The method is to convert the bathymetry into elevation and then combine them together. The DTM was generated from the aerial photos. After we performed the bundle adjustment, we built the stereo pairs in ERDAS Orthomax. The exposure center, the photo position, the ground points and their corresponding conjugate points on the images form a geometric model. Using this model, we derived the 3D shoreline coordinates by measuring the positions of the conjugate points in the stereo pair. After that, we overlapped the DTM with the stereo pair to build a 3-D scene. In this 3D environment, the DTM was edited to correct the errors introduced by conjugate mismatches.

The bathymetry comes in vector format with a scale range from 1:100,000 to 1:2,500. It has one-meter interval counter lines. The bathymetry was registered to NOAA nominal scale 1:80,000 digital vector shoreline. The bathymetry was converted into a grid in Arc/Info. The problem in generating the CTM is that there is a gap between the bathymetry and the land terrain model. This gap was introduced by the resolution and the sampling method used in collecting and generating data.

To fill the gap, the inverse distance method was employed to interpolate the elevation values in the gap. This work was done in Arc/Info. The command used is *topogridtool*. The following steps were used in generating the CTM.

- Transform the projection of bathymetry data into UTM, which is employed as the common projection in this project;
- Calculate elevation from bathymetry. The method is to use bathymetry depth subtracted from the mean sea level, 570.5-Z. the unit is a foot;
- Convert the data unit to the metric system;
- Use the inverse distance method to extend these two data sets, from the DEM toward the water area and from the bathymetry toward the land;
- Overlap these two data sets, and for the overlapping area, take the average of the two as the elevation. Thus, we obtain the CTM.

The DTM has a resolution of 2.5 meters. The original bathymetry is in vector format with an interval of 1 meter in depth/elevation. The bathymetry was converted into grid format with the same resolution as the DTM, 2.5 meters. The bathymetry data has an 1:80,000 map scale. An estimation of two contour intervals error will give 2m of bathymetric error. The estimated accuracy of the CTM is under 4m. A better bathymetric data in the area would definitely help.

3.5 A method for digital shoreline extraction

We generate the digital shoreline through an image processing techniques based approach. Figure 3.4 shows the procedure to generate the shoreline from CTM and water surface data.

The color aerial photos were taken in visible wavelength and the penetrating capacity is low. The DEM in the water area cannot be derived directly from the aerial photos. The *CTM* was generated as described early. The *water surface model* from the GLFS was processed and made available. Similarly, the shoreline should be the contours with the

zero difference value in the resulting model of the *subtraction* of the two surface models. In fact, we used a small range $[-0.1, 0.1]$ as a tolerance to define the shoreline. Furthermore, a *classification* based on the elevation/bathymetry differential values was performed to delineate grid points into land, water, and land-water interaction points and to create a *thematic* image. Subsequently, a *clump* operation grouped the same kinds of grid points together to form clumps of land, water, and land-water interaction areas. After a *noise* detection and deletion process the refined clump image was used to find the shoreline which is defined as one of the boundaries of the clump areas. In the *shoreline detection*, the topology that a shoreline separates water from land was also checked. The raster or grid shoreline was then converted to the *vector shoreline*. Finally, after a visual inspection and editing process, the digital shoreline became available. If the water surface represent the desired MLLW, the derived shoreline is the required *tide-coordinated shoreline*.

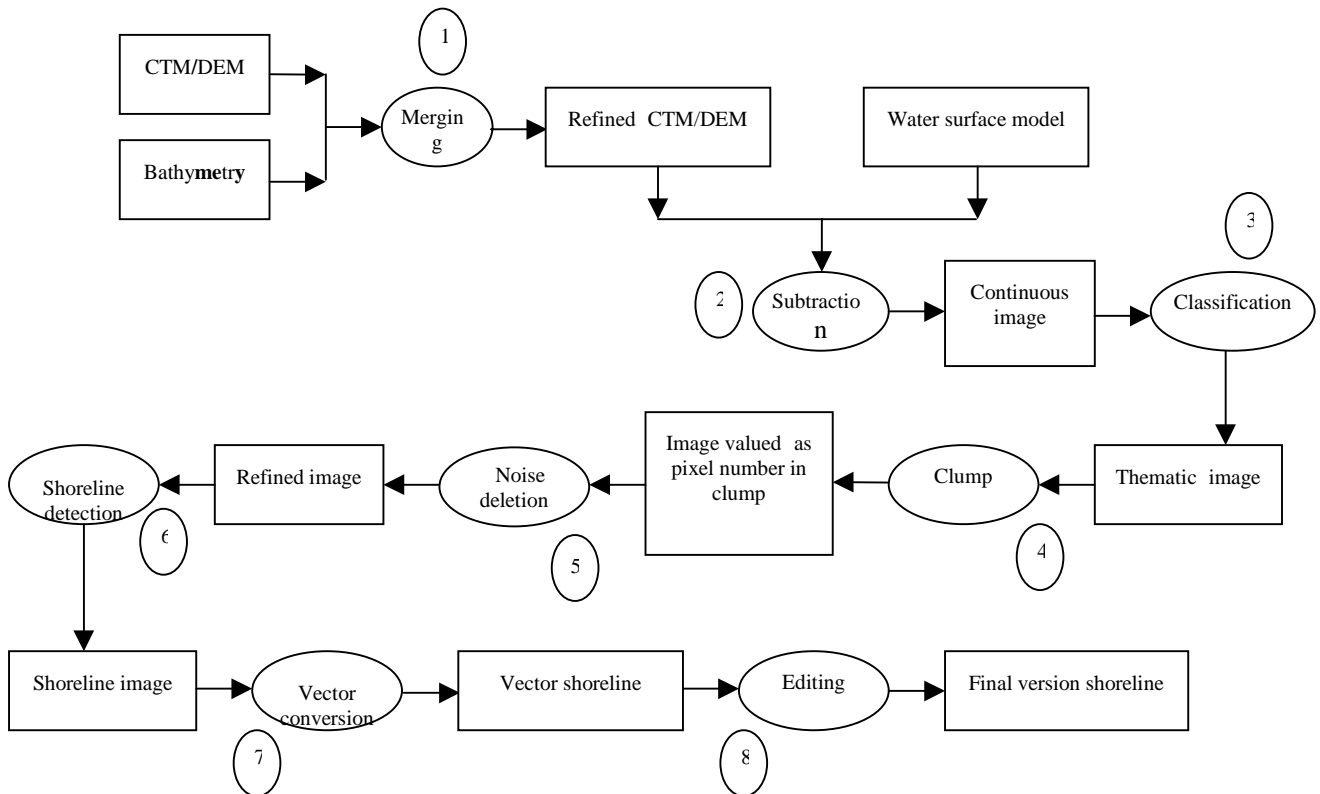


Figure 3.4. Algorithm for generating digital shoreline from a CTM and a water surface

Figure 3.5 shows the intermediate image and the final digital shoreline is shown in Figure 3.6.



Figure 3.5 Candidate area of shoreline

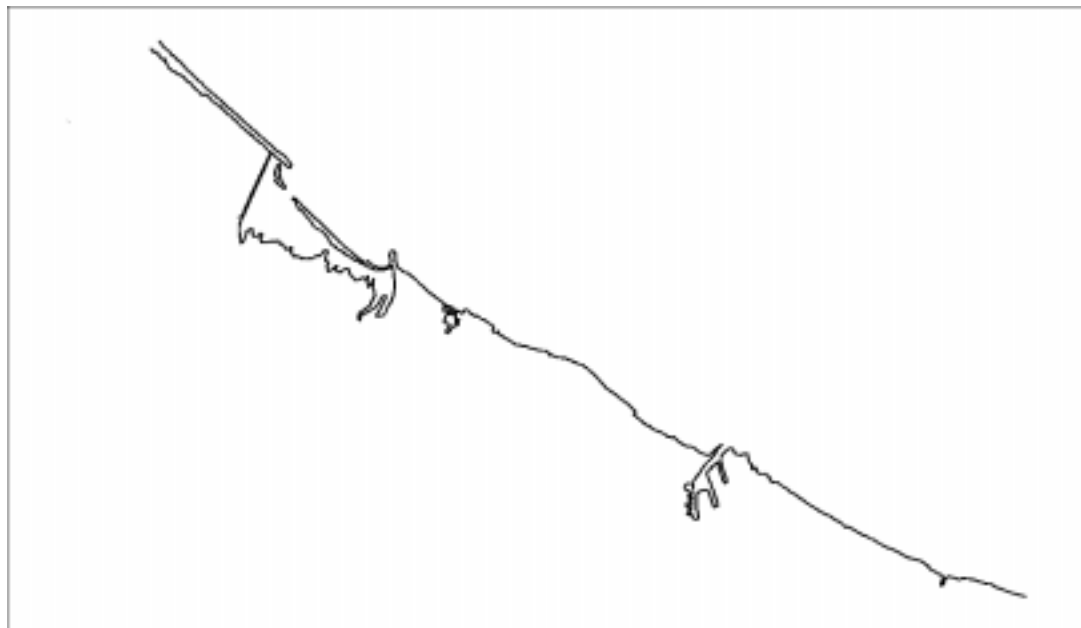


Figure 3.6. The extract digital shoreline

3.6 Accuracy analysis

During the research in this project, we produced three shorelines from orthophoto, simulated IKONOS image and CTM. Together with the available shorelines from USGS, ODNR and NGS/NOAA, we totally have 7 shorelines. We will analyze the accuracy of the shorelines we obtained in our research and talk about the potentiality of digital shoreline generation using CTM.

3.6.1 Shoreline from NOAA T-Sheets

T-sheet is the coastal survey map of NGS/NOAA. It has a scale range from 1:5,000 to 1:40,000. Coastal survey maps are special use planimetric or topographic maps that precisely define the shoreline and alongshore natural and manmade features, such as rocks, bulkheads, jetties, piers, and ramps. Carefully controlled for tide fluxes (standardized to Mean Low Water), these maps represent the most accurate delineation of shoreline in the Nation. Figure 3.7 is an example of t-sheet. Its scale is 1:5,000.

From the standards of NOAA shoreline, the shoreline is defined as the line of contact between the land and a body of water. On Coast and Geodetic Survey nautical charts and surveys the shoreline approximates the mean high water line. In Coast Survey usage the term is considered synonymous with coastline. The shoreline on this t-sheet map is different from those shorelines we obtained. For this map, the mapping error is considered to be 0.5mm on map, which is 2.5 meters on the ground. We take the same error in surveying. So the accuracy of this map is about 3.54 meters. The shoreline is digitized from the digital format T-sheet. The map was scanned in 100 dpi, that means the pixel size on the ground is about 1.27 meters, smaller than 2.5 meters. When we digitize shoreline on this map, we take the digitization error as the same of the mapping error. So the estimated standard deviation of this shoreline is about 4.3 meters. The corresponding errors in X and Y direction are about 3.04 meters.

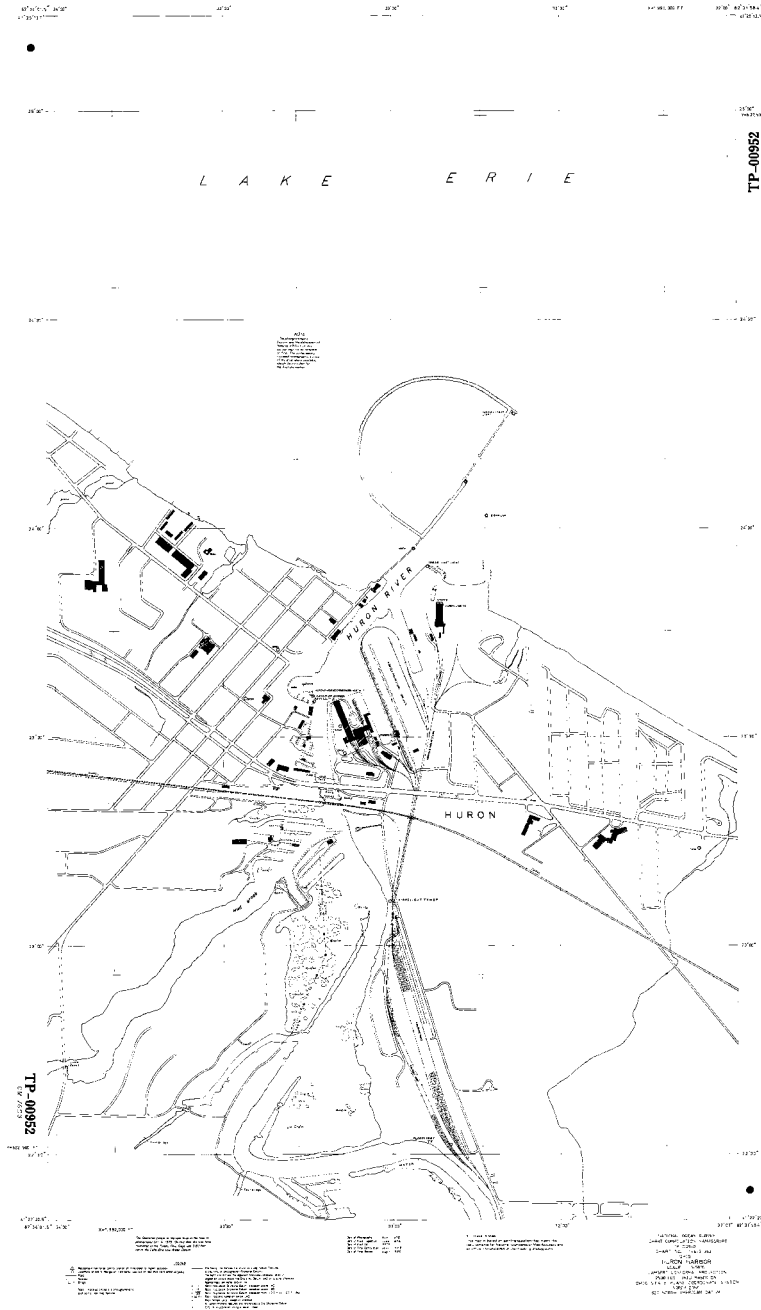


Figure 3.7 T-sheet (Coastal survey map)

3.6.2 Shoreline from USGS DLG

The USGS DLG (Digital Line Graph) has a resolution of 1:24,000. If we take 0.5mm on the map as the mapping error and measure error, its map accuracy is about 12 meters.

If we take the digitalization error the same as the map accuracy, the shoreline from this map has an estimated standard deviation of 20.8 meters. Figure 3.8 shows the shoreline digitized from USGS DLG. It is of 1979.

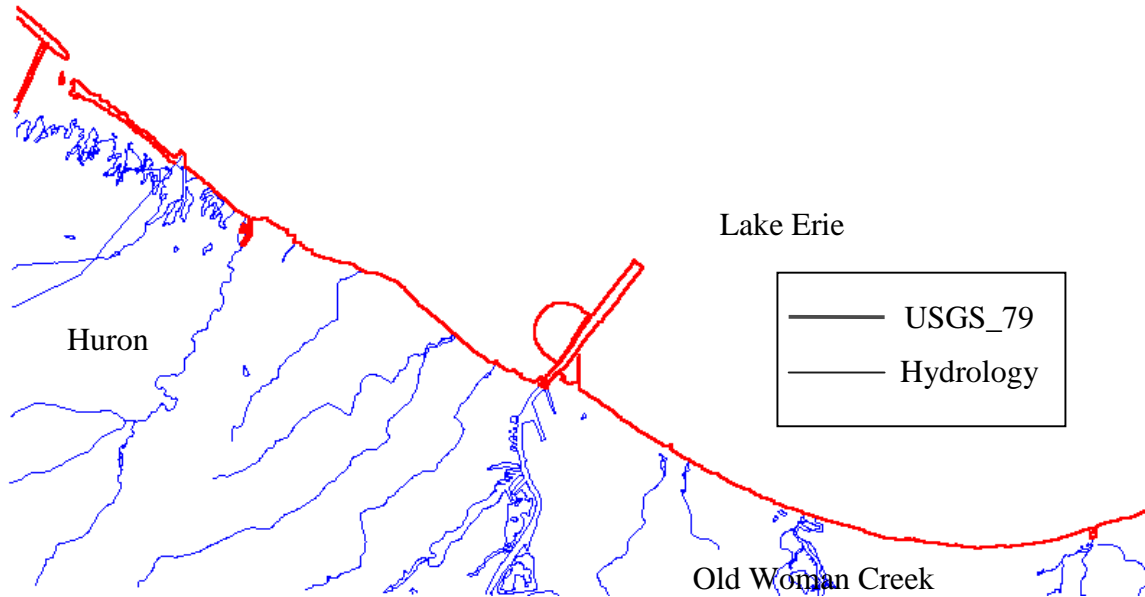


Figure 3.8 Shoreline from USGS

3.6.3 Shoreline from ODNR

When we predict the future shoreline, we need know the recession rate of shoreline. The recession rate are obtained from two shorelines in 1973 and 1990, which were provided by Ohio Department of Natural Resources (ODNR). These two shorelines were compiled from Lake Survey Charts of scale from 1: 4,800 to 1:12,000. We take the accuracy of the smallest scale map, 1:12,000 map, as the accuracy of the base maps. So the estimated standard deviations of those two shorelines in 1973 and 1990 are about 10.4 meters in position. Figure 4.31 shows the two shorelines.

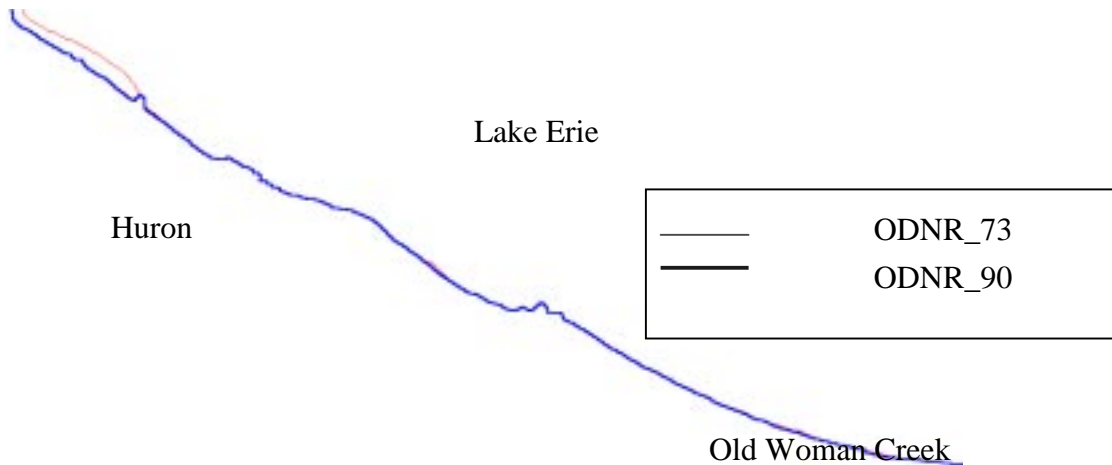


Figure 3.9 Shorelines from ODNR

3.6.4 Shoreline comparison

In this project, we produced three shorelines using different methods and different data resources. One is digitized from the orthophoto, one from the simulated IKONOS images and another from the intersection of the CTM and the water surface model. Table 4.3 shows the estimated accuracies of the shorelines as we analyzed in previous sections. It should be noted that these shoreline accuracies are estimated, instead of being derived by analytical error propagation. In Figure 4.10 are all the shorelines displayed together.

Table 3.2 Shoreline accuracy

Shoreline	Estimated standard deviation
T-sheet	4.3 meters
USGS DLG	20.8 meters
ODNR map	10.4 meters
OSU Orthophoto	2 meters
Digital shoreline	2-4 meters
IKONOS image	2-4 meters

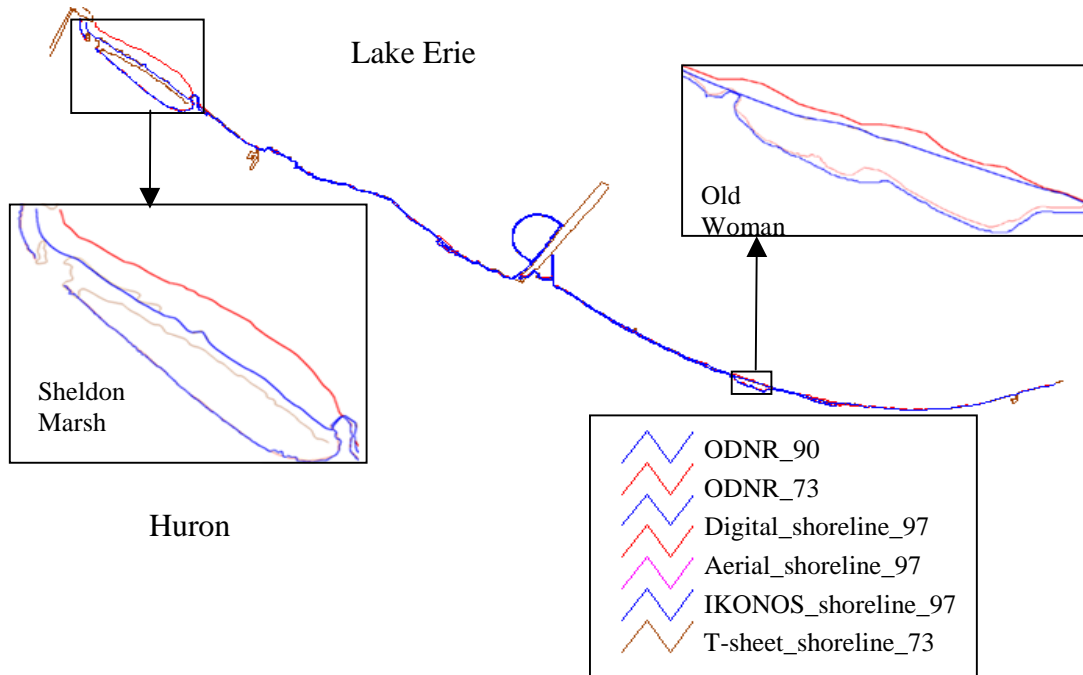


Figure 3.10 Shorelines used in this project

In our project, we studied the methodology to generate instantaneous shorelines using CTM. The method is using the water surface to intersect the CTM. We generated two shorelines using this method. By analyzing the two shorelines, we can see that a small water level change can bring distinguishable shoreline change in horizontal plane especially in small slope areas, which usually is the area having heavy shoreline erosion. See Figure (3.10). By using different water levels to intersect the CTM, we can generate a series of shorelines. Those shorelines can be used to interpolate the tide-coordinate shoreline. From Table 3.2, we can see that the shoreline from CTM has a high accuracy. It is about the accuracy of 1:10,000 scale maps. So this method can widely used in some shoreline applications with a scale of 1:10,000 or smaller. Surely, further study and field tests should be employed before we reach the final conclusion.

In Figure 3.10, we can see that there are large shoreline changes in Sheldon Marsh and Old Woman Creek. In these two areas, the slopes are very small and there is no protection, that means the erosion in these areas is very severe so that the shoreline

changed significantly. Erosion is the main cause of the differences showing in this figure, the coastal materials are sand or clay which is easy to be washed away by the water. The small differences between the digital shoreline and aerial photo derived shoreline may be caused by the water level data and shoreline feature generalization applied by the operator at the time of measurement. As we mentioned before, the water level used in digital shoreline is different from that when the aerial photos were taken.

3.7 Shoreline prediction using linear regression and EPR

Now when we have a method to compute the instantaneous shoreline we can use this method to predict the future shoreline and in a precise way. Figure 4.33 displays the conventional method of predicting shoreline, this is done by a manual End Point Rate (EPR) method on an aerial photograph and with a ruler.

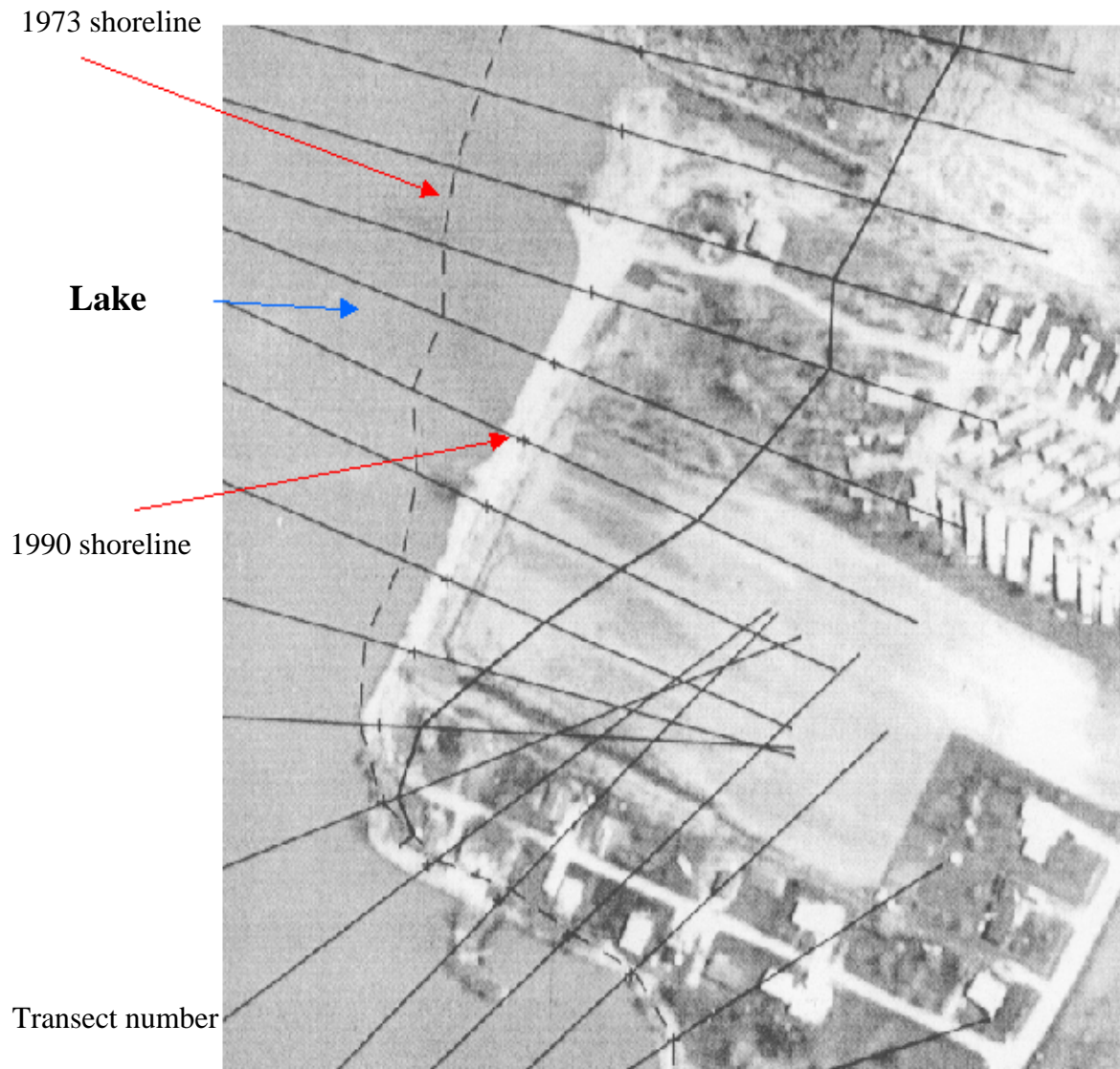


Figure 3.11 Computing erosion rate manually-EPR

To calculate the shoreline in future, several steps were employed to complete the task. First we will automatically compute the distance between the shorelines (those shorelines that we computed using the previous process).

- we convert the previous process file into DXF format and then using Visual Basic program transferred it into X,Y,Z file that we can read in Matlab see appendix 2)
- We first compute the slope of the shoreline 1 between two points as: $m=(y_2-y_1)/(x_2-x_1)$.

- Plot the shorelines for the various years in the same graph.
- Draw perpendiculars from shoreline 1: The slope of this line at that point will be $-1/m$. Using the line equation:
- $y-y_1 = m*(x-x_1)$

We compute the perpendicular line at that point, then draw similar perpendicular lines from various points on shoreline 1 using the corresponding slopes and the X,Y coordinates (Figure 3.12).

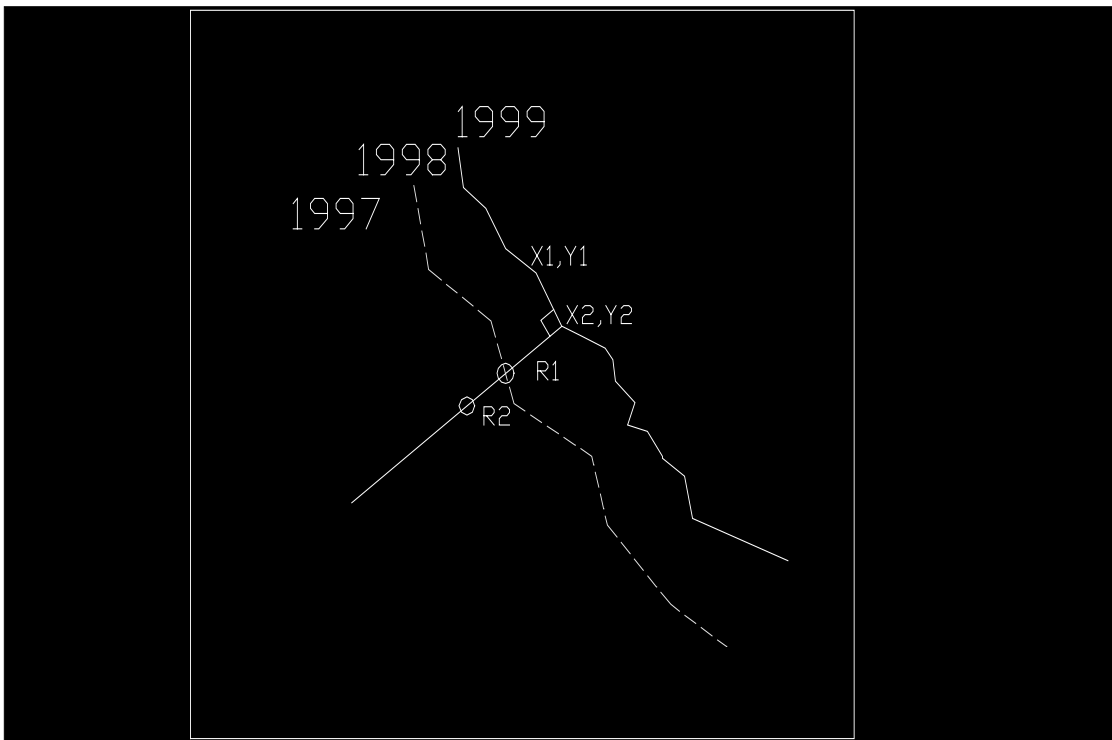


Figure 3.12. Explanation of the method used to compute the distance between shorelines

Since we have already plotted the shorelines for various years on the same graph, we can easily compute the intersection points of these perpendicular lines with the shoreline graphs for the various years – the formula is given below:

If $A_1x + B_1y + C_1 = 0$ and $A_2x + B_2y + C_2 = 0$ are two lines, their intersection point has coordinates

$$X_i = (-C_1B_2 + C_2B_1) / (A_1B_2 - A_2B_1)$$

$$Y_i = (-A_1C_2 + A_2C_1) / (A_1B_2 - A_2B_1)$$

The distances between the intersection points of the perpendicular lines with the shorelines for the various years are then tabulated for each point using the formula:

$$\text{Distance} = \text{sqrt} \left((X_1 + X_2)^2 + (Y_1 + Y_2)^2 \right)$$

We take the mean of these distances and take it as the Rate at that particular point. Figure 3.13 is an example plot produced using matlab.

When we have the distances at a given time (rate) we can predict the shoreline of a particular time in the future.

Rates of Shoreline position changes are frequently employed to summarize historical shoreline movements and to predict the future based on those perceived historical trends. The data used to calculate a shoreline rate of change statistic consist of a number of shoreline positions recorded at one place (e.g. transects or monuments) over time.

Shoreline position data sources include historical maps, maps compiled from aerial photographs and aerial photographs. Each shoreline time/position data point possesses a degree of uncertainty arising from the difficulty of precisely locating the shoreline datum (The mean high water) from shoreline position data sources. A rate of change statistic implicitly assumes that shoreline movement is constant and uniform (i.e. linear).

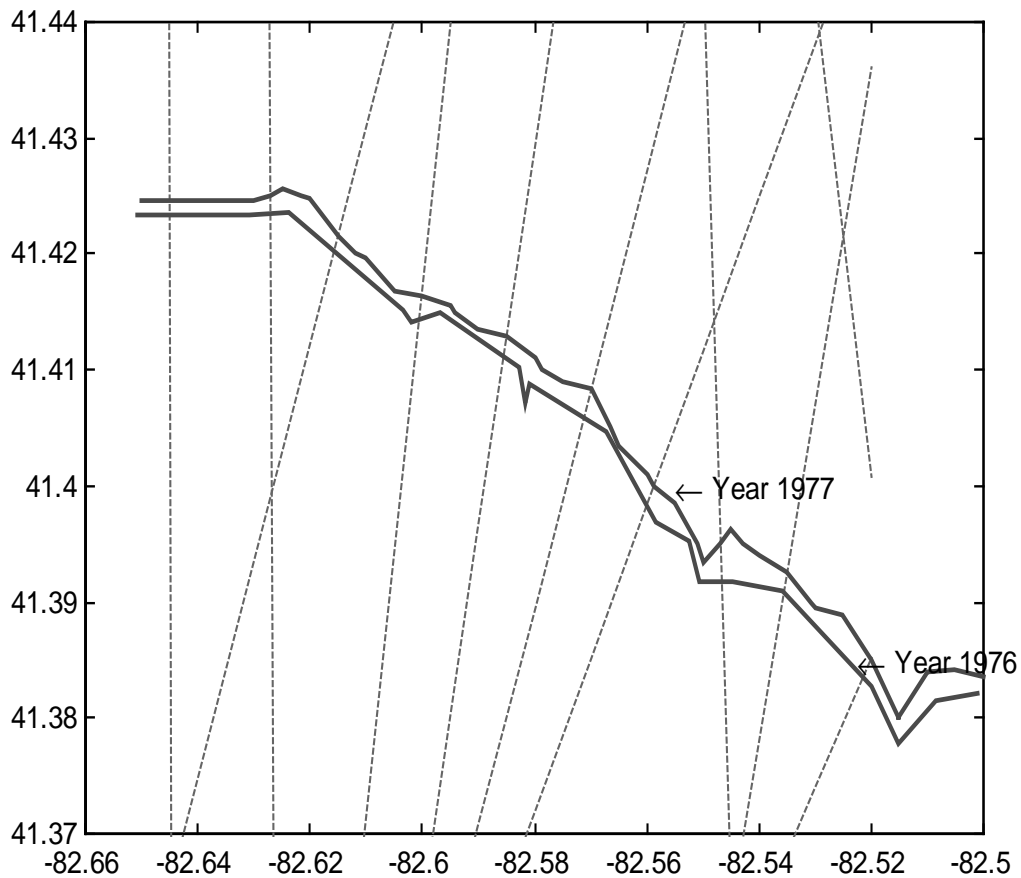


Figure 3.13 An example plot of Matlab output file

Through time, this is in reality, often not the case. Further uncertainty regarding the accuracy of shoreline rate of change predictions thus arises from using linear methods to summarize nonlinear, cyclic, or chaotic shoreline behavior. Several methods have been used to predict beach loss as a function of time or sea level rise. Some of the non-linear method employs complex mathematical models such as higher-order polynomials, exponential, or cyclic series. Nevertheless the method most commonly used, especially by coastal land planners and managers, to predict future shoreline changes is extrapolation of a constant rate-of-change value. The popularity of this method is due chiefly to its simplicity. As with any empirical technique, no knowledge of or theory regarding the sand transport system is required. Instead, the cumulative effect of all the underlying processes is assumed to be captured in the position history.

For the purpose of predicting the future of shoreline positions for study area, simple methods or models have been used, such as the *End-Point Rate* (EPR) method, or *Linear Regression* (LR). Linear regression uses all the available data from many data sets to find the line, which has overall minimum, squared distance to the known points (see Figure 4.36). Until this point in time we could not get a statistically acceptable sample size or span an appropriate time period in order to justify the use of LR model.

The GLFS has all the water level data from the last five years, however, the hundreds of giga bytes are stored in a cassette and are unable to give us the appropriate files. We could get data only of 1997 and 1999. So we used simple EPR model in this research. The future shoreline position for a given date is then estimated using the resulting slope and Y-intercept:

$$\text{Shoreline Position} = \text{Rate} * \text{Date} + \text{Intercept}$$

The EPR model employed a line extracted from the earliest end-point and latest end-point. If we use Y to denote shoreline position, X for date, B for the intercept, and m for rate of shoreline movement, this equation can be simplified as:

$$Y = mX + B$$

Given N shoreline data-sets , numbered in ascending order by date, the EPR is:

$$m_{\text{EPR}} = (Y_n - Y_1) / (X_n - X_1)$$

and the EPR intercept is:

$$B_{\text{EPR}} = Y_1 - m_{\text{EPR}} * X_1 = Y_n - m_{\text{EPR}} * X_n$$

Since the end point line can extend beyond the most recent point (X_n, Y_n), equation (2) can be rewritten to use that position (Y_n), and the elapsed time ($X - X_n$):

$$Y_{EPR} = m_{EPR} * (X - X_n) + Y_n$$

When we picked up the method of shoreline prediction, we can use it because the time between the two data sets we have is too short. We used shorelines collected from Old maps – this was done previously and we had the files from 1973 and 1990. Instead of working again with matlab, we used the Arc/info GIS package where we can use Buffer operation.

The generation of buffer can be based on either a certain distance (constant-width) or a look-up table (variable-width) in Arc/Info™. We eliminated the wrong side of buffer zone after we got it. First, we need to create a look-up table (with the erosion rate at every point) with only two columns; that is, key-item and distance from input coverage. The key-item is Trans (i.e. segment number), and distance is derived from annual recession rate (feet/year) multiplied by 25. Next, we performed buffer function along shoreline coverage and removed lake-ward buffer zone. The result is given in figure 4.37.

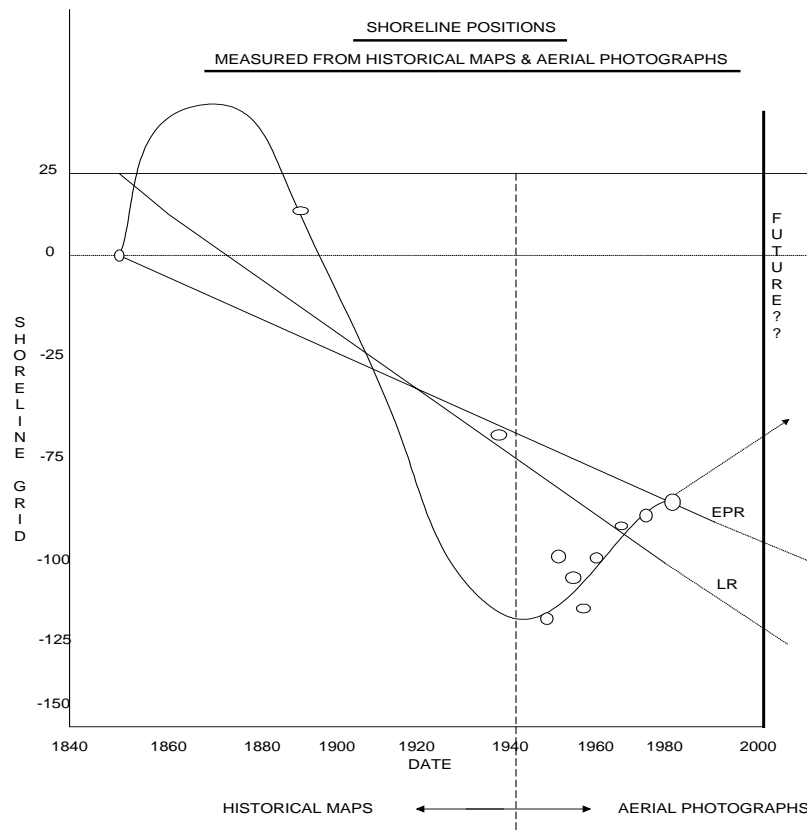


Figure 3.14 Linear regression to compute erosion function

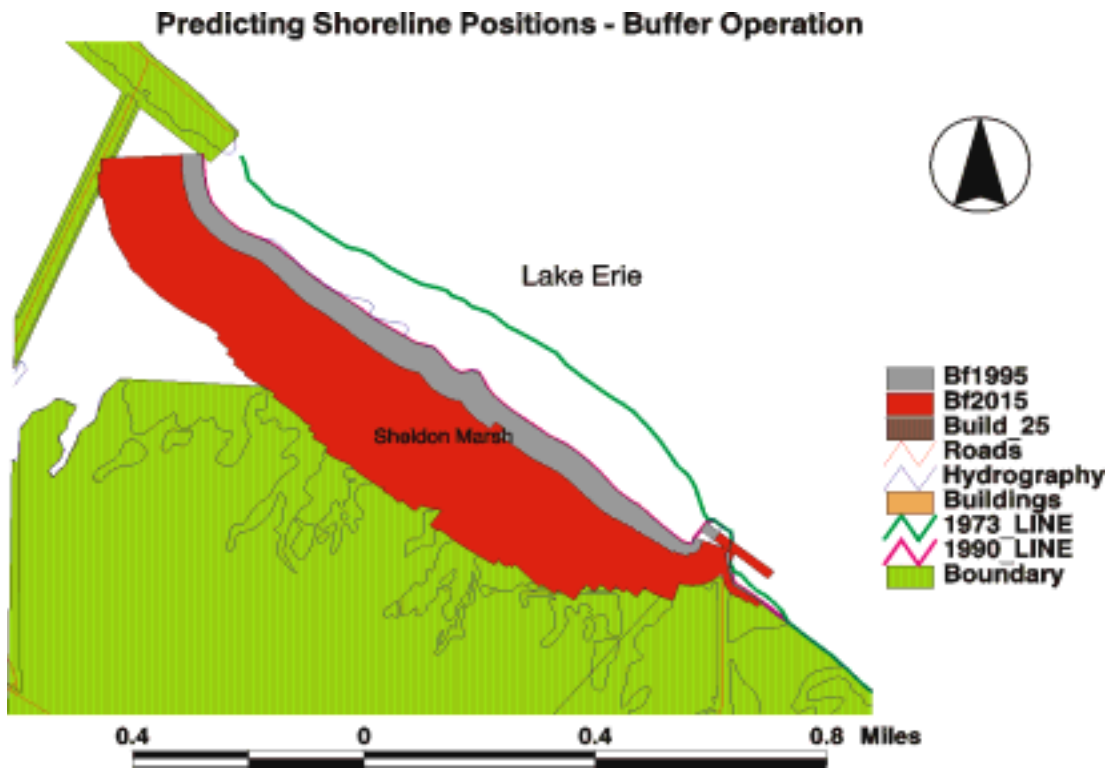


Figure 3.15 An Arc/Info output of predicted shoreline using EPR+Buffer command. Prediction is done to year 2015. Using shoreline from 1990 and 1973.

4. Modeling Shoreline Erosion and Coastal Transported Sediment

In this study, we refer to sediment load resulting from shoreline erosion as direct load into the lake body. The sediment load washed by surface runoffs from the terrain surface and discharged into the lake is classified as indirect load. This is because the shoreline soil loss due to erosion directly discharges into the lake body unlike the surface-originated sediment resulting from surface soil erosion that undergoes a lot of soil-loss-soil-gain processes before it reaches the lake body. The topsoil layer holds some phosphorus from the direct runoffs, which is basically originated from farmlands. In this part of the research we studied both the direct and indirect loads of sediment and phosphorus that discharge into the lake. The soil loss resulting from the erosion that occurred in the southern segment of the Lake Erie shoreline from Sheldon Marsh Preserve to Vermilion in North Ohio in the time period from 1979 to 1997 was studied as direct sediment load. As well, we studied the corresponding phosphorus loads within the eroded soil volume. This time period was chosen according to the data availability. The data sets corresponding to the year 1979 was obtained from the USGS; these were a 7.5-minute DEM and a large-scale DLG converge. These data sets were refined, as reported in detail later, before they were used in this study. The 1997 data set consists of a 2.5-meter DEM and the corresponding orthophotos that we have produced from NOAA Aerial Photos of the study area acquired in 1997. The GIS systems that we have utilized in this study are ESRI's products Arc/Info(7.2.1 & 8.0) and ArcView, and Erdas Imagine.

In this project, one of our goals was to estimate the direct and indirect sediment and phosphorus loads discharged into the lake body and to see to what extent they correlate to each other. This will enable us to better understand the processes that transport the nutrient-enriched sediment during coastal erosion events. We also aimed to study the spatial and physical inter-relationship between the sediment and its corresponding phosphorus mass. We also aimed to derive the concentration of phosphorus in the near-shore zone and to study the correspondence between the land-derived and water-derived phosphorus profiles. To meet these objectives, we carried out the research procedures illustrated in the steps outlined below:

- Estimation of the shoreline soil loss volume in the study period as well as estimation of the total phosphorus loads contained in the eroded soil volume. To get this we computed the soil loss volume between the 1979 and 1997 shorelines after overlaying them on the DEM derived from the NOAA-1997 data.
- Derivation of the phosphorus concentration in the near-shore zone. This was performed through the estimation of the chlorophyll profile which was used to derive the phosphorus profile in the study area near-shore zone.
- Modeling the surface-based sediment load profile and its associated phosphorus concentrations. This was performed only for a sub-basin in the study area, which is the Old Woman Creek (OWC) sub-watershed, because in this area we were only able to gather the all the needed hydrologic, sediment, and phosphorus data.

4.1 GPS field survey

The first step to estimate the erosion caused discharge is to process the NOAA-97 aerial photos and to derive the shoreline in the area. There was a total of twelve colored aerial photos used in the project. Before the processing. We performed a GPS field survey to obtain control points in March 2000. Although two years passed after the photos were taken, most ground features remained unchanged and could match the features in the images very well. Figure 4.1 shows the distribution of the control points measured in the field survey. Because the area covered by those photos is a narrow strip, it is difficult to obtain a good control network. In order to improve the robustness of the network, we observed two more points outside the photo strip. Table 4.1 lists the control points obtained in the field survey.



Figure 4.1. GPS Control points and tie points

Table 4.1. GPS control points

Name	X(m)	Y(m)	Z(m)
AB40	362021.212	4588012.115	175.22
GP01	364725.11	4587902.911	175.783
GP02	363400.474	4585210.519	180.79
GP03	365077.455	4583098.06	104.405
GO04	368695.503	4584860.61	95.072
GP05	367754.754	4581356.358	186.758
GP06	366825.525	4586016.934	170.939
GP07	369975.93	4583671.262	179.63
GP08	372489.384	4582960.908	175.836

GP09	373875.757	4581788.225	183.962
GP10	372963.806	4850460.168	186.661
GP11	369912.496	4581363.752	177.622
COTL	373903.979	4581786.42	184.024
MC10	400395.286	4590898.597	181.899
RMS	0.069	0.057	0.057

4.2 Estimation of shoreline soil-loss volume and the contained phosphorus mass

Using the field survey data, the NOAA aerial photographs were precisely georeferenced. Shorelines were extracted as discussed in former chapters. For estimating the volume of soil loss resulted from shoreline erosion in the period from time t_1 to time t_2 , we have employed a shoreline erosion concept illustrated by the schematic shoreline profile representing the action of the energy flux caused by the breaking waves and currents as shown below in Figure 4.2.

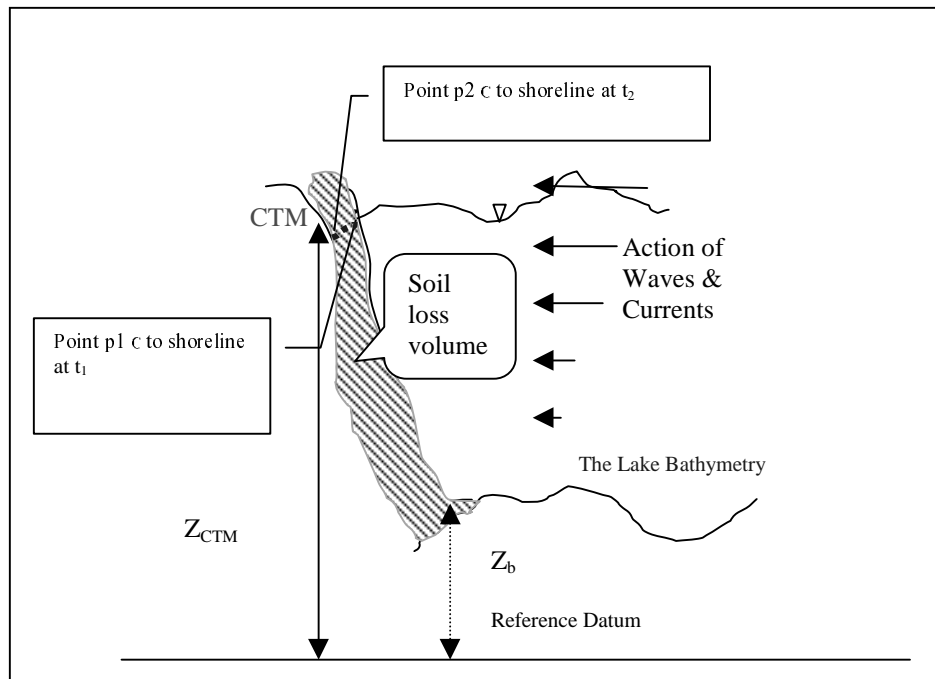


Figure 4.2 Schematic vertical profile of the effect of waves and currents on shoreline

A discrete representation of the coastal sedimentation process based on the conservation of sediment mass principle would result in a discrete version of the conservation equation that has the following form:

$$Q_y = \frac{1}{\Delta t} \cdot \sum_{i=1}^n C_i^2 \cdot D_i \quad (4-1)$$

Where Q_y is the volumetric rate of shoreline soil-loss, n is the number of discrete grid cells that are enclosed between the two shorelines, C_i is the DEM cell size, Δt is the time period, and D_i is the sediment transport zone depth, computed as follows:

$$D_i = Z_{CTM} - Z_b \quad (4-2)$$

Where Z_{CTM} and Z_b are the terrain elevation and the bathymetric height of the i^{th} near-shore cell respectively. As illustrated in Figure 4.1 above, the volume of the soil loss due to shoreline erosion, V can be obtained for each cell using the following formula:

$$V = A \cdot (Z_{CTM} - Z_b) \quad (4-3)$$

where A is the shoreline areal loss. To compute the volume of soil loss, V , and further the volumetric rate of shoreline soil-loss, Q_y , we have implemented the following procedure:

Task1: Resample the USGS-7.5-min DEM to a 2.5-meters cell-size DEM by bilinear interpolation to comply with the CTM-1997 that we have produced in this study.

Task2: Subtract the resampled DEM from the CTM-1997 to produce the coastal loss DEM. Manual editing was performed on the resulted coastal loss DEM since the raster subtraction accuracy is sensitively affected by the DEM resolution.

Tsak3: The models of Equations 4-1 and 4-3 have then been applied on a cell-by-cell basis to obtain the volume of the soil loss due to shoreline erosion and the volumetric rate of shoreline soil-loss, respectively.

At this point it is worthwhile to mention that we have assumed the lake bathymetry remains unchanged through the period of study. Figure 4.3 depicts the soil loss resulted from shoreline erosion in the study area from Sheldon Marsh Preserve to Vermillion along the Southern Lake Erie Shoreline for the study period from 1979 to 1997.

Using Arc/Info[®] and the spatial geo-processing functions in Arc/View[®] and by overlaying the loss area DEM model, the lake bathymetry, and the newly produced DEM from the NOAA aerial photography. Since the bathymetric data were collected before the last state of the shoreline, the bathymetric data do not cover the loss area. For each cell we may have its DEM elevation Z_{CTM} , but not the corresponding depth Z_b in the bathymetric data. Once we have both of them we are able obtain the volume of soil loss using the procedure described above. The procedure to obtain the variables Z_b and Z_{CTM} is described as follows:

- Estimate the bathymetric height Z_b for every cell in the lost coastal zone: for a DEM cell we try to find its nearest bathymetric cells and then calculate the average of the bathymetric depths of both cells; we then assign the average to Z_b ;
- Subtract the value of Z_b from Z_{CTM} to obtained the height of the soil loss volume at each cell; and
- Multiply $(Z_{CTM} - Z_b)$ by the cell area to obtain the volumetric soil loss for each cell and accumulate for the entire soil loss zone to find the total soil loss.

By implementing this method, we found that the soil loss volume in this period for the entire 11km shoreline from Sheldon Marsh to Vermillion is 988,084 cubic feet or 28,035 cubic meters (Figure 4.3). The volumetric rate of shoreline soil-loss, $Q_y=635.54$ ft³/year, is then obtained using the discrete model shown in Equation 4-1 above.

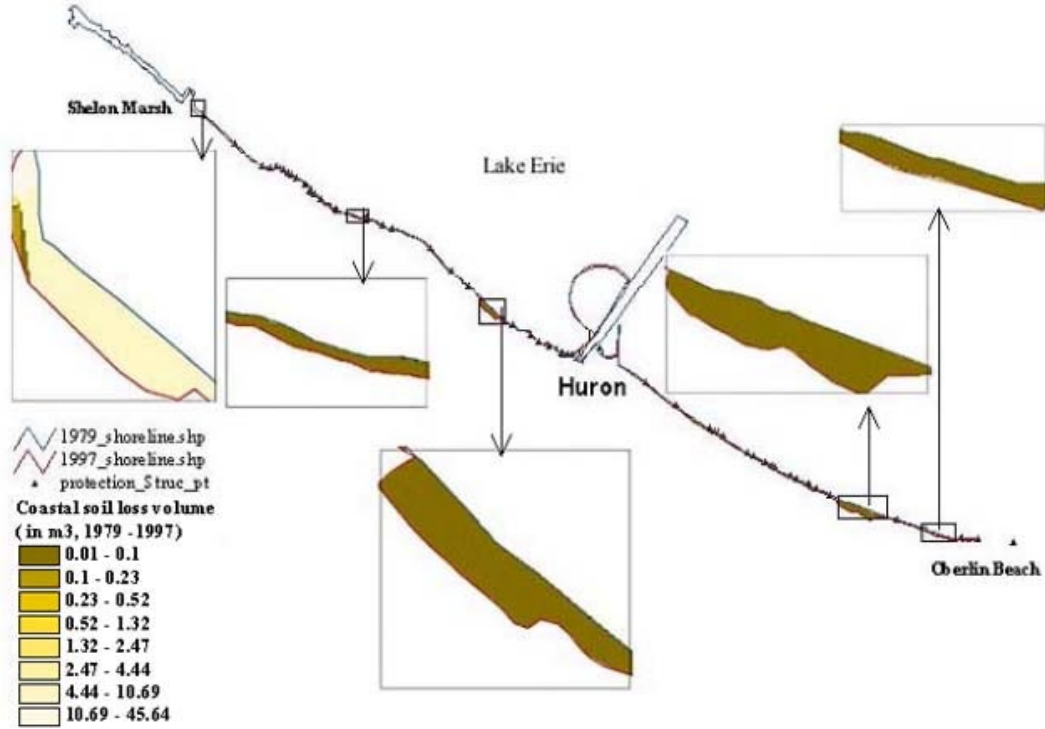


Figure 4.3 The shoreline erosion in the study area from 1979 to 1997

This soil loss volume was then converted into an equivalent potential along-shore sediment transport rate P_l , by using the following relation between volume transport rate Q_l and the immersed weight transport rate I_l presented by Hitoshi and Suzuki (1982):

$$I_l = (\rho_s - \rho) \cdot g \cdot (1 - n) Q_l \quad (4-4)$$

where ρ_s is the mass density of the sediment grains, ρ is the mass density of water, g is the acceleration due to gravity, and n is the in-place sediment porosity ($n \cong 0.4$).

To look deeply into the coastal zone topography in the study area, several spatial cross-shore profiles were generated to study the effect of the spatial pattern on shoreline erosion. As illustrated in Figure 4.4, the shoreline topography for the study area ranges from steep bluffs with abrupt elevation change to gently inclined terrain toward the Lake surface. This complex topography explains the huge soil-loss volume of shoreline due to

erosion by the combined energy flux of waves and currents. This is because the energy flux acts on the toe of the high-rise bluffs resulting in huge shoreline loss.

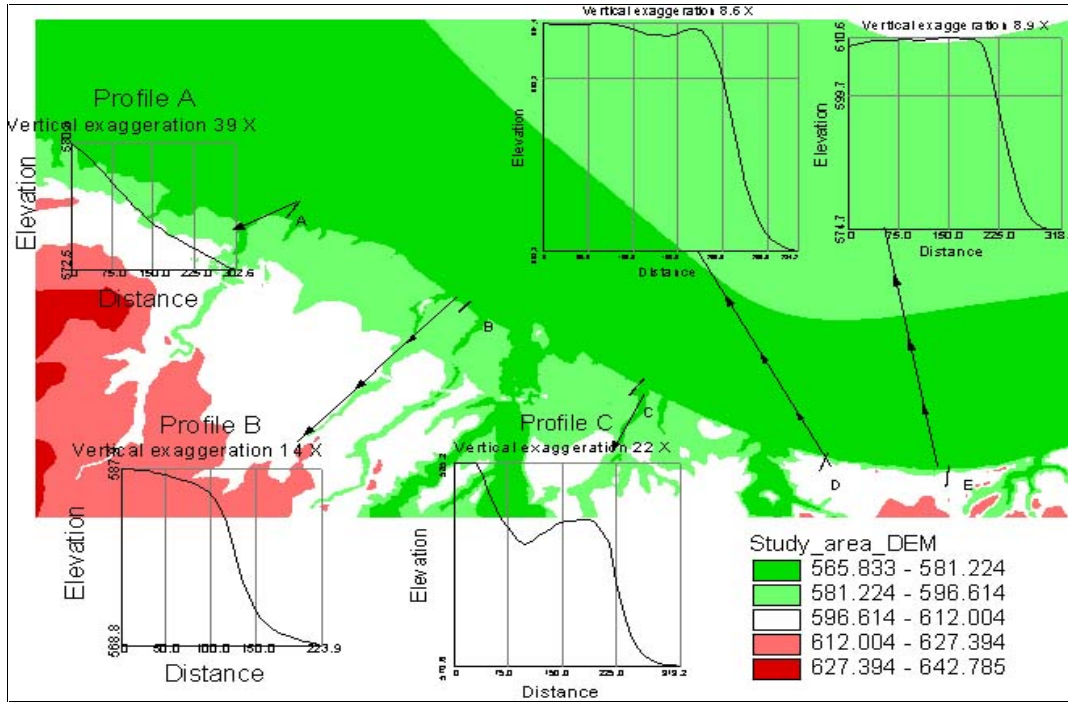


Figure 4.4 Spatial cross-shore profiles in the study area

The effect of the shoreline protection in reducing the shoreline erosion in the area west of the Old Woman Creek (OWC) area is very clear compared to the shoreline piece west of the Creek, which is 60% protected. Figure 4.5 portrays the rigorous shoreline erosion in OWC area generally and at the creek mouth itself in this period of time.

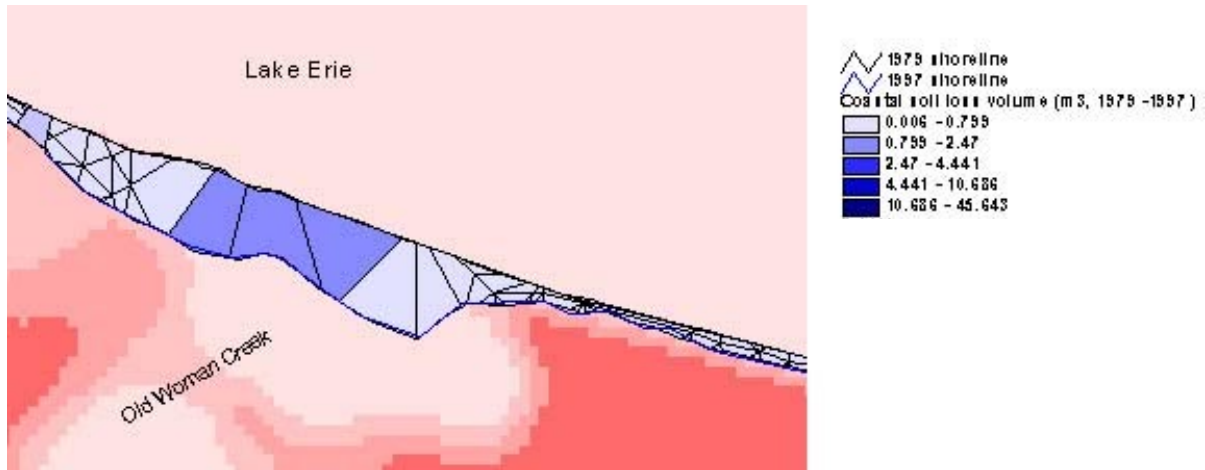


Figure 4.5. A map depicting the eroded shore in the OWC area

The volume of the soil loss estimated for this area was found to be 7,960 cubic feet in the period 1979 to 1997.

4.3 Estimation of the contained phosphorus mass

To estimate the equivalent phosphorus mass in kilograms contained in the volume of shoreline soil loss, we used the results of the runoff-driven phosphorus concentrations based on the expected phosphorus loads corresponds to different land use categories (refer to Chapter 5). The average expected phosphorus load of the 8 g/m³ estimated in the surface modeling part for the OWC study area has then been attributed to the whole coastal soil-loss area (refer to Chapter 5). Using the DEM model for the eroded shoreline on a cell-by-cell basis, we estimated the equivalent phosphorus mass P_{ld} (grams of total phosphorus) contained in the eroded part of the shoreline by implementing the following formula:

$$P_{ld} = 0.23 \cdot A \quad (4-5)$$

where A (in m²) is the aerial coastal soil-loss and the factor 0.23 was obtained by assuming an average expected phosphorus load of 8 g/m³ throughout the whole eroded coastal zone based on the results of the surface phosphorus model (refer to Chapter 5).

Based on this, the contained phosphorus mass was estimated for the whole study area (11km of shoreline) and found to be 744 Kg. This is equivalent to 0.02 mg of phosphorus for every cubic meter of coastal soil loss in the area, which looks insignificant at this level (Figure 4.6).

When we considered factors that effect shoreline erosion, such as the spatial characteristics of the shoreline segments, shoreline protection status, soil type, land use category, and shoreline material, we found that the shoreline protection is the most significant factor that contributes to the erosion stage. The absence of protection structures from a shoreline segment explicitly results in increased shoreline erosion no matter what other factors are involved.

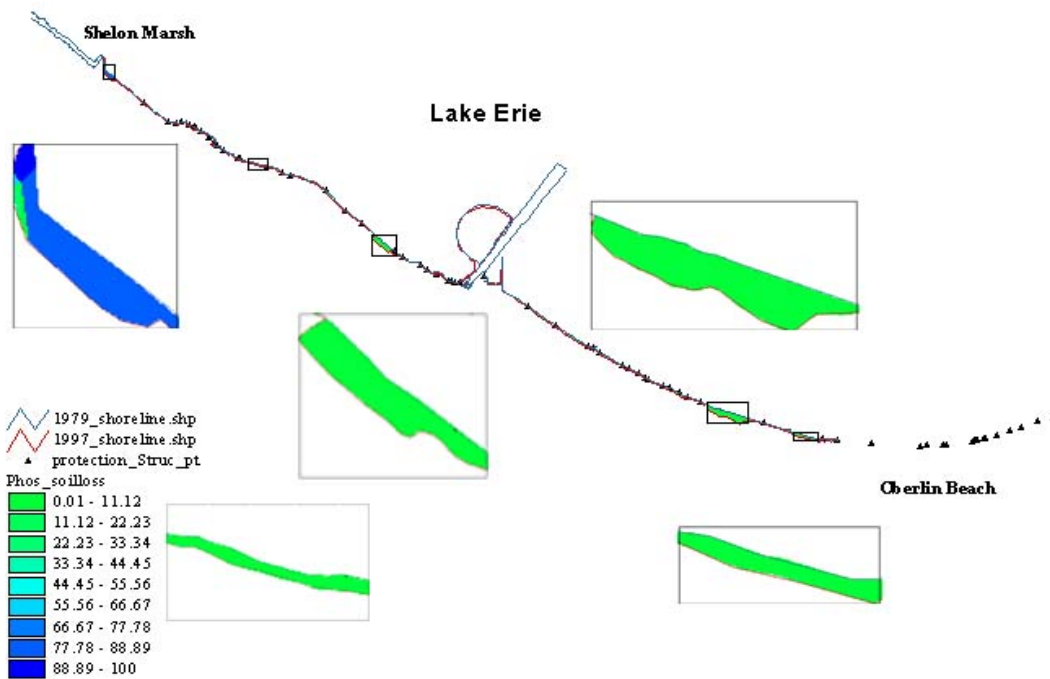


Figure 4.6 The contained phosphorus mass in the shoreline soil-loss volume (1979-1997)

4.4 Derivation of phosphorus concentration in the near-shore zone water

We know that the color of the coastal water column is determined by the interactions of incident light with substances or particles present in the water. The most significant constituents are free-floating photosynthetic organisms and inorganic particulates. The photosynthetic organisms contain chlorophyll, which absorbs light at blue and red wavelengths and transmits in the green. Substances dissolved in water like phosphorus also affect the watercolor. Our goal was to investigate the correspondence and the inter-relationship between the mass of phosphorus discharged into the lake within the eroded shoreline and the amount of dissolved phosphorus in the near-shore zone water.

4.4.1 Coastal water-column reflectance and chlorophyll derivation

The ERDAS Imagine software hyper-spectral analysis functions were employed to estimate the volumetric reflectance in the near-shore zone using the built-in *IAR* model from the NOAA airborne data of 1997. We have created several sub-sets of the imagery so as to analyze only the near-shore zone. This is because we want to identify the corresponding phosphorus-based rather than organic-based chlorophyll concentration. After we computed the volumetric reflectance we used the NASA coastal ocean model (Harding, 1989) to convert our reflectance values to chlorophyll concentrations (mainly *Chl a*):

$$\text{Chl a} = -0.04 + \log_{10} (0.341 - 3.001 * R + 2.811 * R^2 - 2.041 * R^3)$$

where $R = \log_{10} (R_{rs}(490)/R_{rs}(550))$. R is the remote sensing reflectance or the measured radiance corrected from atmospheric effects and normalized for the sun position.

4.4.2 Estimation of the phosphorus

In the literatures several attempts were made successfully to correlate total phosphorus concentrations and chlorophyll levels (mainly *Chl a*), most of which are based on a logarithmic fit (Dillon and Rigler, 1974; Rast and Lee, 1978, and Gakstatter, 1978). We chose the Rast and Lee relation in this study to estimate the corresponding total phosphorus concentrations that correspond to our estimated *Chl a* levels. The Rast and Lee relation is of the form:

$$\text{Log} (chl -a) = 0.76 \times \text{log}(p) - 0.259 \quad (4-6)$$

where *chl-a* is the chlorophyll a concentration in (mg L^{-1}) and *p* is the total phosphorus concentration. We modified this relation to compute the corresponding phosphorus concentrations as shown below:

$$P = 10^{(1.326 \times \text{log} (chl a) + 0.341)} \quad (4-7)$$

The estimated near-shore phosphorus distributions were then converted to a 2.5-meter grid in Arc/Info[®]. The resulting grid was then brought into Arc/View[®] and overlaid with the NOAA bathymetry and the TIN of the terrain aspect that was developed for the area using information from the NOAA-CTM as mentioned previously. We found that, the near-shore model of phosphorus distribution has a value decrease in the offshore direction. The same trend exists in the long-shore direction. This draws the attention to the effect of the bathymetry or, in other words, the effect of the under-water topography on the trend of the near-shore phosphorus distribution. This trend agree with what we were expecting to see assuming that the land is the source of the total phosphorus discharge into the lake body (Figure 4.7). The phosphorus distributions in the Old Woman Creek area are shown in Figure 4.8.

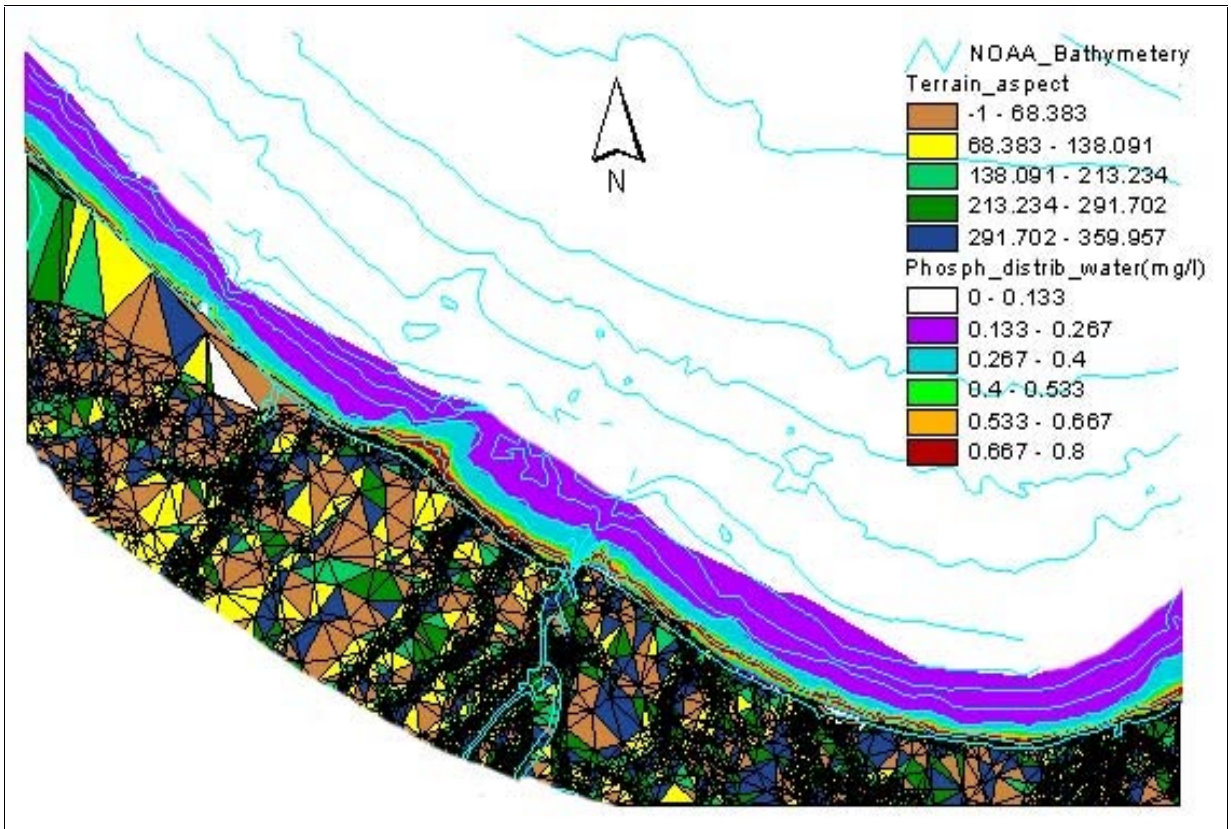


Figure 4.7 The near-shore phosphorus distribution

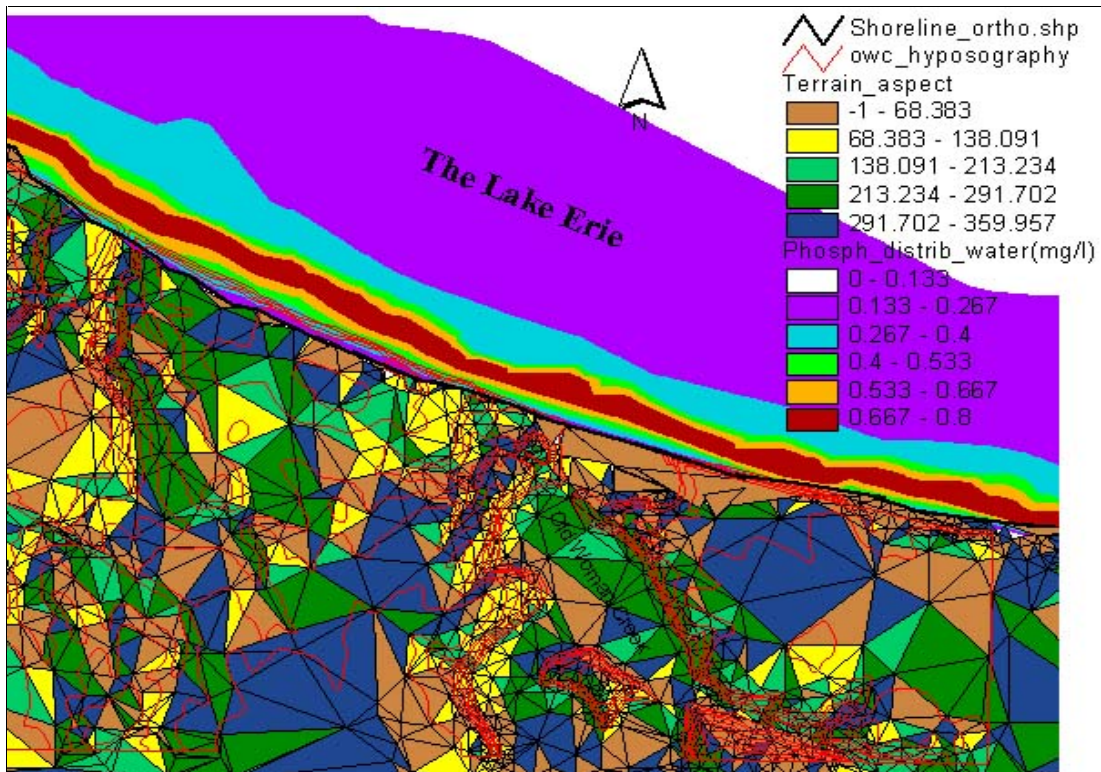


Figure 4.8 The near-shore phosphorus concentration model in the OWC area

5. GIS-based modeling of surface transported contaminated sediment

The surface flow digital modeling performed in this study was partly based on the approach described by Greenlee (1987), and Jenson and Domingue (1988) and all tasks were completed in the Arc/Info[®] GIS system. The only exception is that we did not use the flow-accumulation method, solely because we think it should not assume that all cells in the flow-direction model have the same hydrologic characteristics. This is because surface runoff is not only based on the terrain topographic characteristics, but is also based on the hydrologic characteristics of the soil as well as on the land use category and the cover condition. Therefore, we think that the standard procedure of Arc/Info[®] for establishing a flow-accumulation model has to incorporate information about the hydrologic characteristics of the soil surface. This means the procedure used to calculate the flow-accumulation should not treat all cells as if they had the same runoff potential.

The surface erosion model in this study was performed only for the Old Woman Creek basin (OWC), which is just a part of the whole research area, for the reason that the hydrologic functions are based on the delineation of the hydrologic boundaries of the study area. These are not pre-identified boundaries and they depend very much on the terrain topography and the spatial interaction among the spatial entities. Another reason is that we want the scale of the study to be as large as possible, to better understand the complex environmental phenomena under study. Therefore, the following environmental modeling was performed just in the OWC extent.

5.1 Digital GIS-based Modeling of the Old Woman Creek Area

The basic digital elevation model used for this study is the USGS 7.5-minute DEM, which has a 30m square cell size. A second one has been developed in this research using a NOAA-1997 data set of aerial photos and ground control points acquired through a GPS survey conducted by our research team. The latter DEM has a 2.5-m cell size. Most

processing stages were done using Arc/Info[®] Version 7.2.1 GRID module, Erdas[®] imagine, Matlab[®] and Math-Cad[®], and ArcView[®].

The USGS DEM downloaded from the Internet should be corrected for data errors that exist in the original data file, before digitally simulated stream networks can be created. In particular, raw digital elevation models downloaded from Internet may contain many sinks. Sinks are single grid cells or groups of cells surrounded by cells of higher elevation. Arc/Info's *fill* command is used to remove these sinks. The *fill* command redefines the elevations of each of the sink points to be equal to that of its lowest elevation neighbor. This smoothing process is usually applied to digital elevation models after re-projection operations. That is because of the data re-sampling process that has taken place during the re-projection operation, which often creates such sinks in the DEM or the grid.

Once the filled hydrologic digital elevation models have been created, they can be processed to determine the direction of the flow of water from cell to cell and to determine, for each cell in the grid, the number of cells that are upstream together with information about their potential runoff coefficients. This modified method generates a float grid instead of an integer grid. The standard *flow-direction* procedure implemented in many GIS systems has the shortage of the physical representation of the runoff process as it just considers topography as the limiting factor for the determination of the directions of surface flow. The basis of this process relies on the 8-neighbor concept (Greenlee, 1987; Jensen, 1987). The output of the *flowdirection* function is an integer grid whose values range from 1 to 255 (Figure 5.1). If a cell is lower than its 8 neighbors, that cell is given the value of its lowest neighbor and flow is defined towards this cell. If multiple neighbors have the lowest value the cell is still given this value, but flow is defined with one of the two methods explained below. If a cell has the same change in z value in multiple directions and that cell is part of a sink, the flow direction is referred to as undefined. In such cases, the value for that cell in the output flow-direction grid will be the sum of those directions. For example, if the change in z value is the same both to the right (flow direction =1) and down (flow direction = 4), the flow direction for that cell

is $1 + 4 = 5$. Cells with undefined flow direction can be flagged as sinks using the SINK function.

64	128	1
32	X	2
16	8	4

Figure 5.1. The x-cell-8-neighbor concept

A digital representation of the stream network in the study area is established by generating the accumulated surface flow in the creek and streams after incorporating information about the runoff variation characteristics by means of the runoff coefficient. This was done by generating a runoff coefficient grid based on the hydrologic classification of the soils in the study area as well as the land uses. This runoff coefficient grid was then merged with the flow-direction grid after both were converted to a polygon coverage using the *gridpoly* command. This task incorporates all the possible factors that have an effect on the potential runoff from every cell in the flow-direction model, which will help in creating an accurate flow-accumulation model in the next step. The Arc/Info *conditional* function was then implemented to extract from the estimated potential runoff model the cells that have value greater than a certain threshold, which was set to 300 for this study. The resulting raster model shows cells whose flow accumulation values are greater than the 300 thresholds. The flow accumulation cells with value greater than 300 are extracted to define the locations of the digitally simulated stream coverage *hydrcov1*. In order to digitally delineate drainage areas, outlet cells for the study area should first be established. This is done through Arc/Info Grid module, by displaying the flow accumulation grid, overlaying the *gage_point* coverage, and selecting the gage location along the flow accumulation grid. This is done by *selectpoint* command that allows users to interactively define the outlet points. Once the outlet cell grid is defined, the drainage boundaries for the study area could be created using the *watershed* function, along with

the flow direction grid, to define the area draining to the selected cell. An equivalent coverage of the drainage area is then created using the *gridpoly* command.

As we mentioned previously, the method of hydrologic digital modeling, which has been implemented in Arc/Info[®] as a standard procedure based on (Greenlee, 1987 and Jensen, 1988) had some deficiencies. We therefore modified the standard Arc/Info[®] hydrologic modeling procedures by incorporating the terrain hydrologic characteristics into our modeling procedures through the utilization of the widely used un-calibrated rational method (RM). We first utilized the RM to estimate the watershed area that contributes runoff to the gage station at the Old Woman Creek and US route 6 for examination purposes, by comparing it to our results using the digital approach. We also used the runoff coefficient (RC) concept to produce an improved flow-direction model using land uses in the study area before the runoff model was generated accurately. This guarantees a better hydrologic representation for the study area terrain surface since topography is not the only factor that influences the surface runoff.

5.2 Correlating the digitally-estimated and measured runoff volumes

In order to evaluate the amount of surface sediment and phosphorus in the study area, an understanding of the means by which the loads move is required. Nutrient enriched sediment is carried over the land surface to water bodies by means of surface flow or runoff, which results from precipitation. By matching the average stream flow at the USGS flow gage in the study area with the digitally estimated runoff that is being assumed to occur upstream of the gage station, a mathematical relationship between rainfall and runoff is obtained. The Parameter-elevation Regressions on Independent Slopes Model (PRISM), discussed in the data presentation and preparation section, provided the precipitation data used for this study. This data is provided as monthly and annual depth of precipitation in millimeters (mm) averaged over the 30-year period from 1961 to 1990.

To calculate the runoff volumes from the study area, the average daily stream flow values of the USGS stream flow gage station at Berlin Road, which is located at the south border of the study area, are subtracted from the values of the USGS stream gage station at Old Woman Creek to accurately generate the runoff volume that corresponds to the study area. The measured stream flows for these gage stations are available for the period 1987-1993 only from the USGS database. Using the values for the annual surface runoff obtained using the modified flow accumulation method mentioned previously, and the values for measured 6-year average annual depth of stream flows at the gage stations, regression analysis was performed to determine the best-fit curve between the two data sets. This was a regression analysis by the *least squares* method for fitting a line to a set of observations. Assessments of the best linear, best quadratic, and best exponential fit show that the linear relationship accurately represents the estimated and the measured runoffs relationship for the study area. The correlation coefficient was found to be 0.995, which indicates that the best-fit line approximates the actual data well. Based on the regression output, the linear relationship that best approximates the rainfall-runoff relationship in the study area is of the form:

$$Q = 0.79 \cdot P - 1.65 \quad (5-1)$$

where Q represents the depth of modeled runoff and P represents the estimated cell-based runoff depth, both in millimeters (mm). In order to create an Arc/Info grid of modeled runoff, this relationship would be applied to every cell in the estimated-runoff model. However, since the precipitation grid has an effective range of values between 1.75 mm and 3.75 mm, it is noted that there is a small range of cells that is less than or equal to 2.0 mm for which the relationship produces negative numbers. In order to avoid that, this relationship was only applied to estimated runoff model cells with value greater than 2.1 mm. Rewriting Equation 5-1, the model finally looks like:

$$Q = 0.79x P - 1.65, \quad P > 2.1\text{-mm} \quad (5-2)$$

The limitation of this modeling function results in runoff values of $Q = 0$ or even negative for precipitation values that are less than or equal to 2.1mm. The study area receives more than 2.1mm when considering the grid-based model results. This will only affect the resulted runoff values when we consider the measured precipitation values for January and February, which are both equal to 1.75mm. Therefore, the adjusted linear model results are acceptable as long as we will be using the grid-based model values. The reason for this is that runoff happens only after surface soils reach a saturation state and also because runoff varies over time with rainfall events. Moreover, there are further factors that influence the runoff event, as we mentioned previously, even if we have more precipitation in one site compared to another. These include the topsoil saturation point, the cover condition, the moisture content in the topsoil layer, and the land use. As these factors make the derived runoff model more adequate. Using this modeled runoff relationship in connection with the precipitation grids and Arc/Info *conditional* statement, grids of runoff can be produced. Then the subsequent flow accumulations may be performed on this grid without encountering cells of no-data value. The *IsNull* command is used with a second *conditional* statement to fill all the no-data cells resulting from applying this model on the cell-level with zeros.

To model the runoff from ice melting, we have treated the ice-sheet thickness as equivalent to precipitation depth, but without a reduction coefficient since the top-layer of the soil is basically saturated, so the whole ice-sheet depth is contributing to the runoff. Based on our results from the precipitation-based surface runoff analysis, we assumed that to have ice-based runoff, the effective ice-sheet thickness should not be less than 2.1 mm. Consequently, the runoff depth Q_s (mm) resulting from an ice-sheet that has a thickness I_d (mm) that is greater than 2.1 mm is given by:

$$Q_s = I_d - 1.65 \quad (5-3)$$

5.3 Modeling the phosphorus intensity distribution in the OWC coastal area

The phosphorus level that occurs during runoff events is measured in terms of the expected mean concentration, defined as the mass of phosphorus transported per volume of runoff. The resulting phosphorus loading coverage as a function of land use categories includes seven expected concentrations for each land use category within the research area. This was created using an advection-driven mathematical relationship (Chapra, 1997 and McCuen, 1998):

$$\text{Loading (W)} = \text{concentration (C)} \times \text{Runoff (Q)} \quad (5-4)$$

Of course, using such a relation assumes a dispersion-free system. The validity of this assumption depends on how large the deviation of the average runoff and average phosphorus intensity are from the discrete runoff and phosphorus values on the cell level. The expected phosphorus concentrations used in this study resulted from a previous National Estuary Program analysis (Baird et al., 1996) that defined a specific phosphorus concentration for every land use category in the study area. These data were used after being adjusted with results of a phosphorus analysis study of major soil series in the Lake Erie Basin (T. J. Logan, 1989). The procedure of using the land uses or soil characteristics to predict the nutrient intensity is an approach that has been adopted in the literature by many researchers (Omernik, 1976 and McCuen, 1998), but our interest here is to study the effect of topography on the distribution of total phosphorus in the study area for better coastal management.

The phosphorus loading that each cell contributes to the study area outlet was estimated by taking the product of the expected phosphorus concentration and the runoff depth corresponding to that cell, as shown in Equation 5-4 above. An assumption is made here before adopting this approach to get phosphorus loading at the study area outlet. This assumption is that no phosphorus consumption occurs during the course of flow to the outlet. This is an appropriate assumption for this study when we consider that the size of the research area is small, which obviously results in short flow-paths. Subsequently,

the cell-based phosphorus-loading model was established as a product of the expected concentration grids and the runoff grids. Figure 5.2 shows the estimated annual phosphorus load model for the OWC area.

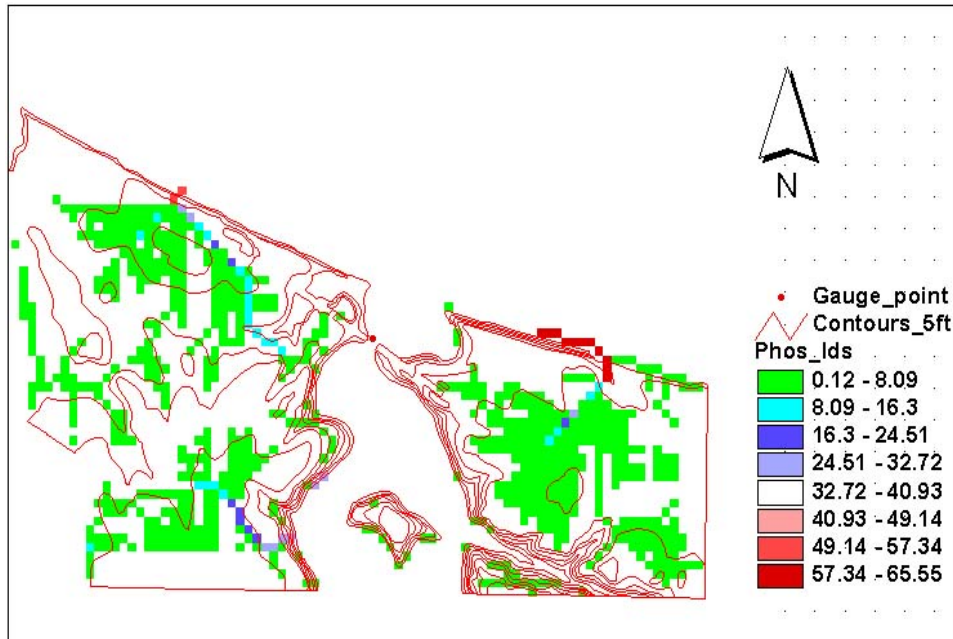


Figure 5.2. The estimated phosphorus-loading model for the OWC (g/m^3)

This model shows that most of the total phosphorus load comes from the northeastern portion of the study area, where agricultural land uses are prevalent, and we can see clearly that even within these agricultural land uses and in a very small spatial extent, the phosphorus concentration still varies. The expected spatial and temporal mean concentration value from a broad perspective of all land uses in the study area seems to be in the range of 0.12 to $8.09 \text{ g}/\text{m}^3$. This value indicates that all or most of the expected mean concentrations are higher than the reporting limit for total phosphorus for all land uses in the study area. This indicates that almost all farmers in the study area adopt the same fertilizer management program except in relatively small sized portions of the study area. Based on the distribution maps, the expected phosphorus model also illustrates a weak correlation between the expected phosphorus loads and the land use categories. This highlights the following points (Figures 5.3, 5.4, and 5.5):

- Employing land use as a index to predict the expected phosphorus loads in this study area may not be the best method since the correlation between them in this area is not as strong as that with other factors such as topography;
- The estimated typical phosphorus load with surface runoff from this study area regardless of land uses or other factors is 8 g/m^3 ; and
- We found a strong correlation between the terrain type and the phosphorus concentration. For example, a steep terrain surface increases the phosphorus load since the complex terrain surface produces higher surface runoff with fluctuating flow velocities that result in increased surface washing.

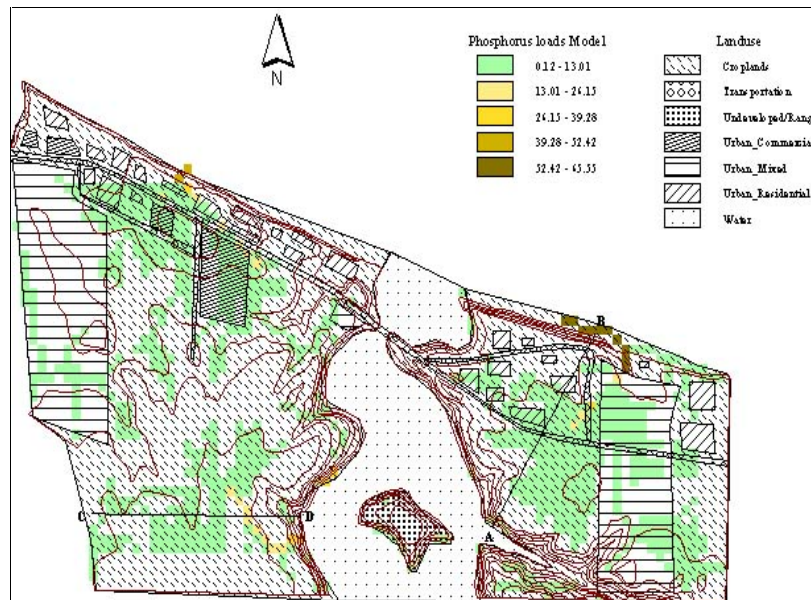


Figure 5.3. The estimated phosphorus-loading model and land-uses in OWC area

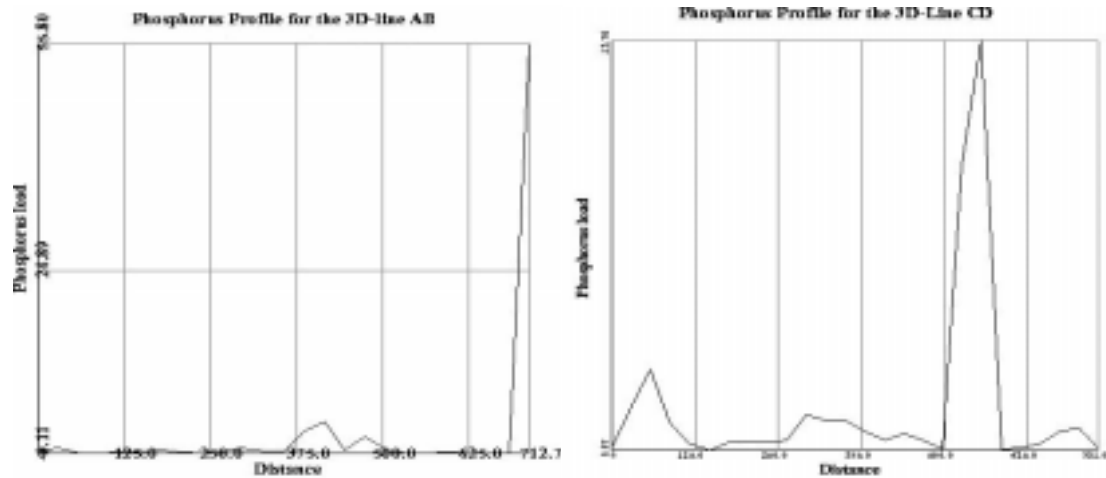


Figure 5.4. Total phosphorus-loading profiles along lines AB & CD of Figure 5.3.

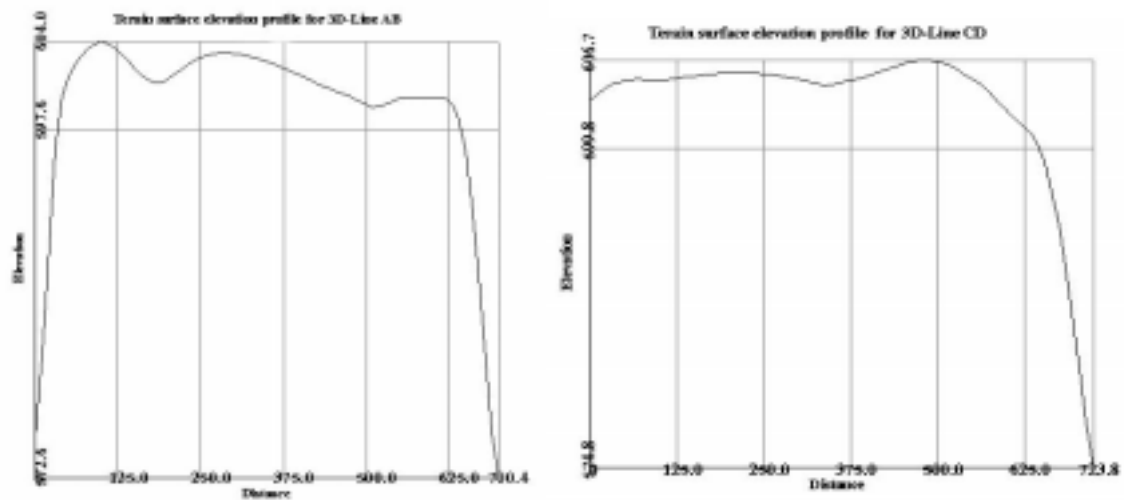


Figure 5.5. Terrain-surface elevation profiles along lines AB & CD of Figure 5.3.

5.4 Soil loss Modeling using the Revised Universal Soil Loss Equation (RUSLE)

We were interested in estimating the eroded surface-soil mass, which acts as available input element for the surface runoff to convert it to transported sediment. To derive this basic input element for the sedimentation process, we adopted the widely used Revised Universal Soil Loss Equation (RUSLE). RUSLE is a surface erosion model designed to

predict the monthly and annual soil loss (E) carried by runoff from specific field slopes in specified cropping and management systems as well as from rangeland. It is also applicable to non-agricultural conditions such as construction sites. Numerical values of its five factors are derived from analysis of research data from National Weather Service precipitation records. For most conditions in the United States, the approximate values of the factors for any particular site may be obtained from charts and tables in the RUSLE handbook (Agriculture Handbook Number 703, USDA, 1997). The RUSLE computer program would also be a good choice for those who would like to directly integrate RUSLE DOS output into their digital databases. Soil loss due to water erosion is modeled in this study using the Revised Universal Soil Loss Equation (RUSLE), which computes both the average monthly and annual expected erosion in the study area. It has the general form:

$$E = C \times R \times K \times LS \times P \quad (5-5)$$

where E is soil erosion in ton/ha, C is a dimensionless cover management factor, R is the average annual rainfall erosivity factor, K is the soil erodibility, LS is the slope length and steepness factor, and P is the erosion support practice factor.

Using the USDA RUSLE DOS program, the five erosion parameters shown above are obtained considering the local characteristics of the study area. These include; soil series and other soil characteristics, surface texture, crops cultivated in the area, rotations, and the average soil slopes. The values for these factors have been linked to the digital elevation model of the study area. Monthly and annual grids of soil loss due to water erosion were also established.

5.5 Determination of the erosion-sedimentation relationship

In this study, the volume of runoff from a grid-cell is completely attributed to precipitation over the cell. By comparing the average sediment loads at the USGS flow gage in the study area with the average soil loss that occurs upstream of the gage as have

been obtained above using RUSLE, a mathematical relationship between soil loss and soil gain is obtained.

The method used for calculating average soil loss for this study is the same method used for modeling rainfall, which uses the modified flow accumulation technique. For this study, soil erosion grids resulting from the RUSLE model are used as weight grids to generate grids that represent monthly and total annual sediment flow corresponding to the study area. To calculate the actual amount of soil loss from the study area in terms of amounts of transported sediment, the average daily sediment loads obtained from the USGS suspended sediment database, as explained above, are used in this study. The idea used here to estimate the actual amounts of soil loss from the study area is very simple. The measured amounts of sediment loads at the gage station were treated the same way as estimated runoff to establish a mathematical relationship between sediment loads and eroded soils, in order to determine the actual amounts of eroded soils. It is shown that the third degree polynomial best fits the relationship between the recorded sediment loads and the eroded soils that are estimated using RUSLE (Figure 5.6).

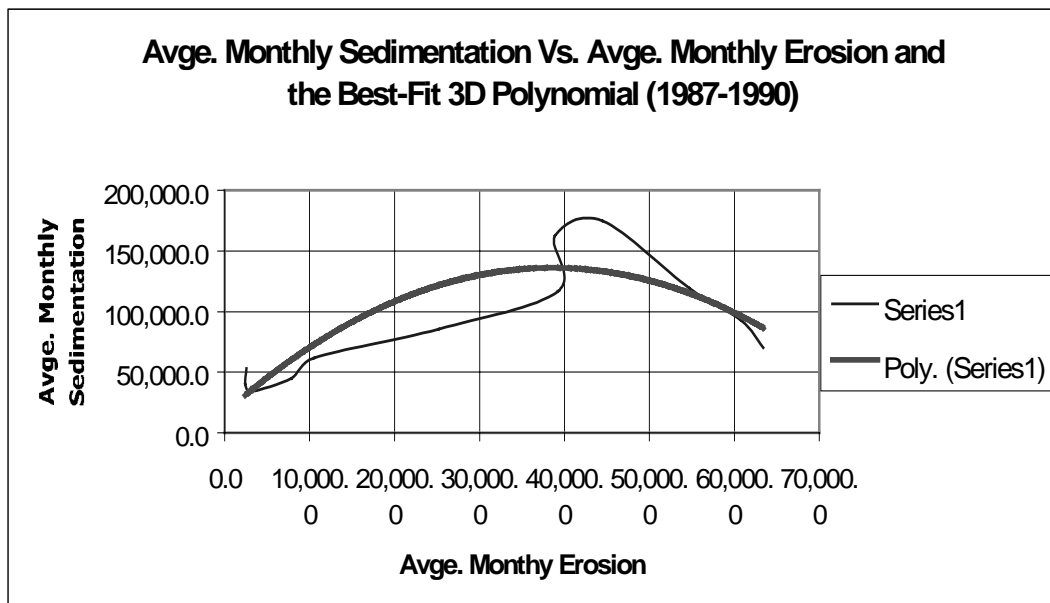


Figure 5.6 The average monthly sediment load, monthly weighted soil loss due to erosion, and the best-fit Polynomial

The correlation coefficient was found to be 0.98, which indicates that this third order polynomial approximates the actual data sets to an acceptable extent. Based on the least squares solution, the polynomial that approximates the Sediment Loads-Eroded Soil relationship in the study area is of the form:

$$S = a_0 + a_1 \cdot E + a_2 \cdot E^2 + a_3 \cdot E^3 \quad (5-6)$$

where S represents the mass of actual soil loss as measured at the gage station in units of kg and E represents the mass of eroded soils as estimated using RUSLE in units of kg. The residuals have been estimated and found to be in the range from 3.742 to 380 grams of soil. A residual analysis shows that February has the highest sedimentation value and November has the lowest, while June, which has a residual of 0.136, is comparatively high. In order to create an Arc/Info grid of actual soil loss, this relationship needs to be applied to every cell in the erosion grids. Using the relationship of Equation 5-6 in association with the erosion grids and the Arc/Info *conditional* statement, grids of actual soil loss are produced. The *IsNull* command is used with a second *conditional* statement to fill all the no-data cells resulting from application of the eroded soil-actual lost soil relationship with zeros. Then, equivalent annual and monthly coverages of actual soil loss are created using the *gridpoly* command.

Figure 5.7 depicts the resulting soil-loss model, that is, the actual transported sediment obtained for the OWC basin. On this figure, the actual soil loss volumes are comparatively small in the northwestern parts of the study area for the reason that the Lake Erie shore there is completely protected, reducing the actual volume of transported sediment as a result of soil erosion. It should also be noticed that the croplands in the south parts the study area contribute heavily to the actual soil loss volumes (Ali and Li, 2000).

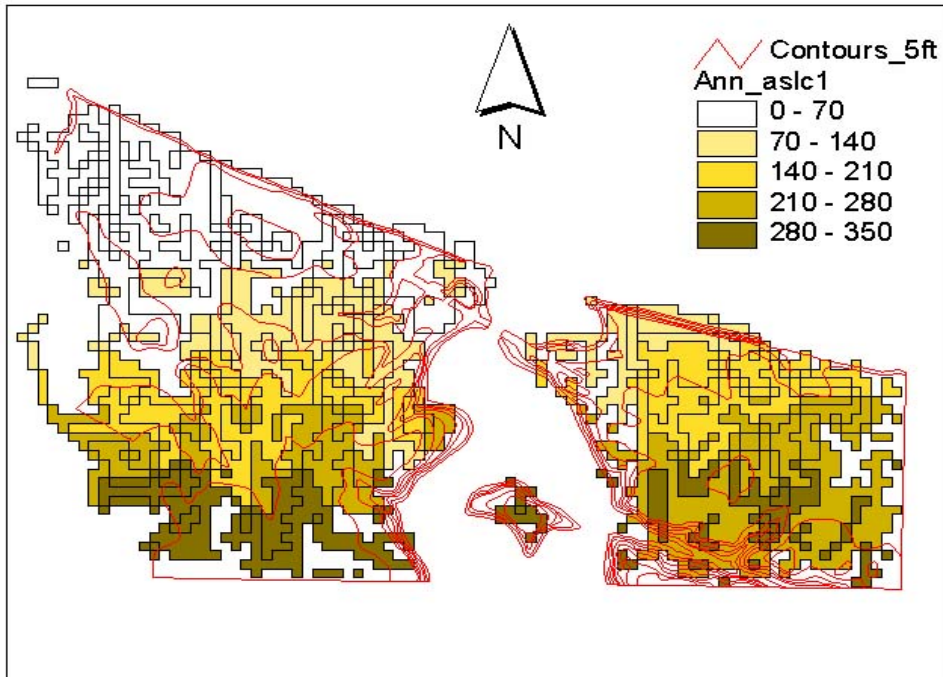


Figure 5.7 Erosion-based sediment model for the OWC area

5.6 Model Consistence Assessment

Since both the soil loss model (surface sedimentation model) and the phosphorus model we developed in this study were based on the runoff model, we therefore need to assess the consistency of the runoff model. To check the consistency of our surface runoff model we utilized the widely used un-calibrated rational method (RM). It is recognized that soil properties vary spatially (both in X and Y). Soil hydrologic characteristics however vary in depth (Z). In this study we are concerned about the 3D variation of soil properties that influence both the surface runoff and soil detachment.

In view of the importance of the hydrologic characteristics of soils on the runoff volumetric rate, the U.S. Soil Conservation Service (SCS) classified U.S. soils on the basis of their runoff potential and grouped them into four hydrologic groups that are either A, B, C, or D. The SCS furthermore developed a runoff curve number (CN) as an

index that represents the combination of hydrologic soil group, land use, and treatment class. The CN therefore gives the possible runoff as a function of soil group, land use and moisture content. The RM uses a runoff coefficient (C) that is approximately equivalent to the CN discussed previously. The RM relates the peak runoff discharge (Q, ft³/sec), the basin area (A, acres), the rainfall intensity (i, in./hr), and the runoff coefficient (C):

$$Q = C \cdot i \cdot A \quad (5-7)$$

The runoff coefficient is a function of the land use, cover condition, soil type or soil group, and the watershed slope. To estimate the runoff discharge from our basin we need to re-write the RM equation in the discrete form shown below:

$$Q_m = \sum_{i=1}^n q = \sum_{i=1}^n \frac{C_i \cdot i_i \cdot a_i}{3600} \quad (5-8)$$

where Q_m is the average runoff volume in (ft³) for the period of study, q is the runoff from every cell in (ft³), C_i is the runoff coefficient for the cell i , a_i is the i^{th} cell area (in acres), and i_i is the rainfall depth in the i^{th} cell in (inches). We need this discrete form of the RM equation to compute the total runoff using the precipitation depth obtained from the PRISM model, the cell area, which is 900m², and the cell-based runoff coefficient as input. The Arc/Info *gridpoly* command was used to convert the annual precipitation depth grid to a polygon coverage before being merged with the soil-type coverage. The soil-type coverage mentioned above is the one that was originally created using the soil map we obtained from the Erie Soil and Water Conservation District in Sandusky, Ohio. The average runoff depth in mm was obtained for all the cells in the study area using the discretized-RM-model of Equation 5-8 above and the runoff coefficients taken from McCuen, 1998 for the 7-land use categories that we have in our study area.

$$Q_m = \sum_{i=1}^7 q = 3.991(mm) \quad (5-9)$$

The estimated average annual value of runoff, Q_m from our model was found to be 3.79mm, whereas the average annual measured runoff value estimated for the gage record in the period from 1987 to 1990 was found to be 3.8 mm. This means that our runoff model underestimated the measured runoff with a discrepancy of 1% from the measured value while the discrete RM approach overestimates the runoff volume by more than 4%. We believe that the underestimation discrepancy found in our model is reasonable.

6. Conclusions

This research project developed and demonstrated a method that uses high-resolution satellite images to precisely map the Ohio Lake Erie shoreline and shoreline changes. Through the project of an 11km shoreline from Sheldon Marsh to Vermilion, Ohio we showed the potential of this new technology for mapping the entire shoreline and shoreline changes of Ohio Lake Erie.

The shoreline change monitoring methods developed are effective in quantifying the coastal erosion and environmental changes caused thereby. Based on the accurate observations, a new approach has been developed to characterize and monitor the direct transport of nutrient-enriched sediments, including phosphorus, during the coastal erosion processes. GIS-based models have been developed in this study that can estimate cell-based runoff depth, eroded soil-based phosphorus mass, and indirect surface soil transported sediment.

There is farming practice in the project area, east of OWC. However, the results show that the phosphorus load caused by farming in this area is not significant comparing to the majority of the non farming area. We found that a weak correlation exists between the phosphorus distribution and land use in the OWC area. We also found that the total coastal sediment budget consists mainly of the eroded volume of the shoreline, while the total phosphorus budget consists principally of the indirect phosphorus load washed by the surface runoff.

The distribution of land-based phosphorus is affected by the coastal terrain topography. Accordingly, we found that the water-column phosphorus distribution that was derived from the coastal chlorophyll profile is to some extent influenced by the lake bathymetry. To efficiently model the surface runoff, a proper representation of the hydrologic characteristics of the terrain soil-types must developed to incorporate both the topographic and hydrologic characteristics.

Acknowledgment

At first we would like to thank Dr. Keith Bedford for his unlimited cooperation and we extend our thanks to his research group members especially Dr. Philip Chu. We also appreciate the assistance and cooperation of Dr. David Schwab of the GLERL of NOAA in Ann Arbor, MI. We also thank staff at the Ohio State Center For Mapping (CFM) for their help with the GPS receivers, especially Dr. Dorota Grejner-Brzezinska. Our appreciation extends to Dr. C. E. Herdendorf at the Department of Geological Sciences of the Ohio State University for his unlimited assistance and for his generous cooperation. We also appreciate the continuous support and help from Dr. Scudder Mackey and John Watkins of the Ohio Department of Natural Resources in Sandusky, Ohio.

We thank Dr. David Klarer of the Old Woman Creek Research Center and Brent Kuenzli of the Ohio EPA at Bowling Green, Ohio. Thanks go to Nancy Funni of the Erie Soil and Water Conservation District in Sandusky, Ohio. Discussions on processing of IKONOS imagery with Dr. Xinghe Yang and Dr. Younian Wang are appreciated very much. A great appreciation extends to the Ohio Lake Erie Protection Fund (LEPF) for funding this project.

References

Alamus, R., M. Langner, and W. Kresse 2000, Accuracy Potential of Point Measurements in MOMS-Images Using a Rigorous Model and a Rational Function. International Archives of Photogrammetry and Remote Sensing, 33(B4), Amsterdam, pp. 515-517.

Ali, T. 1999, GIS modeling of Phosphorus Concentration, soil loss due to Water erosion and Coastal Terrain Change Detection in Lake Erie Coastal Areas, MS. thesis, The Ohio State University, 88 pp.

Ali, T. and R. Li 2000, Spatio-temporal Modeling of Soil Erosion and Contaminated Sediment Transport in Lake Erie Coastal Area, ASPRS Annual Conference, Washington, D.C., May 22-26, 2000 (CD-ROM).

Baird, F.C., T.J. Dybala, M.E. Jennings and D.J. Ockerman 1996, Characterization of Non-point Sources and Loadings to Corpus Christi Bay National Estuary Program Study Area; Corpus Christi Bay National Estuary Program, Corpus Christi, TX.

Bartsch, A. F. and J. H. Gakstatter 1978, Management Decisions for Lake Systems on a Survey of Trophic Status, Limiting Nutrients, and Nutrient Loadings in American Soviet Symposium on use of Mathematical Models to Optimize Water Quality Management, EPA-Office of Research and Development, Environmental Research Laboratory, FL, EPA-600/9-78-024, pp. 372-394.

Bedford, K. and D. Schwab, 1990, Preparation of Real-Time Great Lakes Forecasts, CRAY CHANNELS, Cray Res. Inc., MN, 12 (2), pp. 14-17.

Bedford, K. and D. Schwab, 1991, The Great Lakes Forecasting System - Lake Erie Nowcasts/Forecasts. Proc., Marine Technology Society Annual conference (MTS '91), Marine Technology Society, Washington, DC, pp. 260-264.

Belorgey, M. and R.D. Rajaona et al 1993, Sediment Transport Mechanisms in Coastal Environments and Rivers, Cambridge, UK.

Blumberg, A. F. and G. L. Mellor, 1987, A Description of a Three-Dimensional Coastal Ocean Circulation Model, Three-Dimensional Coastal Ocean Models, Ed. N. Heaps, American Geophysical Union, Washington, DC, 4, pp. 1-16.

Bossler, J.D. 1996, Airborne Integrated Mapping System, GIM, July, pp. 32-35.

Brown, L.C. and T.O. Barnwell 1987, The Enhanced Stream Water Quality Model QUAL2E and QUAL2E-UNCAS: Documentation and User Manual, EPA/600/3- 87/039, U.S. Environmental Protection Agency, Athens, GA.

Brüggemann, B.M and O. Horstmann 1995, Rechnergestützte Bearbeitung von Projekten des Küsteningenieurwesens, In: V. Berkhahn & M. Olbrich (eds.): Forum Bauinformatik Hannover 95 Düsseldorf: VDI-Verlag, Reihe 20, Nr. 173.

Burrough, P.B. 1996, Opportunities and limitations of GIS-based modeling of solute transport at the regional scale. ASA-CSSA-SSSA Bouyoucos Conference, Mission Inn, Riverside, CA, USA, May 1-3 1995, paper title 'Applications of GIS to the modeling of non-point source pollutants in the vadose zone'.

Carter, H. and D. Guy 1980, Lake Erie Shore Erosion and Flooding, Erie and Sandusky Counties, OHIO: Setting, Process, and Recession Rates From 1877 to 1973, 129 pp.

Carter, R.W.G. 1988, Coastal environments: an introduction to the physical ecological and cultural systems of coastlines. Academic Press, London.

- Chapra, S. C. 1997, Surface water-quality Modeling, McGraw-Hill, New York.
- Cheng, P. and T. Toutin 2000, Orthorectification of IKONOS Data Using Rational Function. Proceeding of ASPRS Annual Convention, Washington D.C., May 22-26, 2000.
- Chow, V.T., D.R. Maidment and L.W. Mays 1988, Applied Hydrology, McGraw-Hill, Inc., New York.
- Collins, M.A. and R.O. Dickey 1989, Stochastic Modeling of the Rainfall Runoff-Process for Non-point Source Pollutant Load Estimation, Texas Water Resources Institute College Station, TX.
- Daly, C., R. Neilson and D. Phillips 1994, A Statistical-Topographic Model for Mapping Climatological Precipitation over Mountainous Terrain, Journal of Applied Meteorology, 33, pp.140-158.
- Dillon, P. J. and F.H. Rigler 1974, the phosphorus-chlorophyll Relationship for Lakes, Limnology and Oceanography, 19, pp. 767-773.
- Dowman, I. and J. Dolloff 2000, An Evaluation of Rational Functions for Photogrammetric Restitution, International Archives of Photogrammetry and Remote Sensing, 33(B3), Amsterdam, pp. 254-266.
- Ebner, H. and G. Strunz 1988, Combined Point Determination Using Digital Terrain Models As Control Information, International Archives of Photogrammetry and Remote Sensing, 27(B11), pp. III/578- 587.
- Ebner, H., T. Ohlhof and E. Putz 1996, Orientation of MOMS-02/D2 and MOMS-2P Imagery, International Archives of Photogrammetry and Remote Sensing, XXXI (B2), pp. 158- 164.

Ebner, H., W. Kornus and G. Strunz 1991, A Simulation Study on Point Determination Using MOMS-02/ D2 imagery, *International Journal of Photogrammetric Engineering and Remote Sensing*, 57(10), pp.1315-1320.

Ebner, H., W. Kornus and T. Ohlhof 1992, A Simulation Study on Point Determination For The MOMS-02/D2 Space Project Using An Extended Functional Model, *Int. Arch. Of Photogrammetry and Remote Sensing*, 29(B4), pp.458- 464.

Erie County Soil Survey Book 1971, U.S. Department of Agriculture Soil Conservation Service, Ohio Department of Natural Resources Division of lands and soil and Ohio Agricultural Research And Development Center.

ESRI 1991, *Arc/Info Use's Guide V. 6.0, Arc/Info Data Model, Concept, & Key Terms*.

ESRI 1992a, *Arc/Info User's Guide V. 6.0, Dynamic Segmentation, Modeling Linear Features*.

ESRI 1992b, *Arc/Info Use's Guide V. 6.1, GRID Command References*.

ESRI 1997, *Understanding GIS The Arc/Info Method, Self-Study Workbook, Version 7.1 for Unix and Windows NT*.

Foster, G.R. and L.D. Meyer 1975, *Mathematical Simulation of Upland Erosion by Fundamental Erosion Mechanics, Present and Prospective Technology for Predicting Sediment Yields and Sources Proc., Sediment Yield Workshop, USDA Sediment Lab., 285 pp.*

Frank, A. U. and D. M. Mark 1991, *Languages issues for GIS: Principles and Applications*, edited by Maguire, D. J., Goodchild, M. F. and D. W. Rhind, 1, pp. 147-163, Long man Scientific and Technical Inc.

Fraser, C. and J. Shao 1996, Exterior Orientation Determination of MOMS-02 Three-Line Imagery, Experiences with the Australian Testified Area, International Archives of Photogrammetry and Remote Sensing, XXXI (B3), pp.207-214.

Fritsch, D., M. Kiefner, D. Stallman and M. Hahn 1998, Improvement of the Automatic MOMS02-P DTM Reconstruction, International Archive of Photogrammetry and Remote Sensing, GIS-Between Visions and Applications, Stuttgart, Germany, 32(4), pp.170-175.

Fritz, L. W. 1996, Commercial Earth Observation Satellites, International Archives of Photogrammetry and Remote Sensing, ISPRS Commission IV, pp. 273-282.

Goodchild, M.F. 1992, Geographical information science, The International Journal of Geographical Information Systems, 6(1), pp. 31-45.

Greenlee, D. 1987, Raster and Vector Processing for Scanned Linework, Photogrammetric Engineering and Remote Sensing, 53(10), pp. 1383-1387.

Habib, A. and B. Beshah 1997, Modeling Panoramic Linear Array Scanner, Department of Civil and Environmental Engineering and Geodetic Science, The Ohio State University, Columbus, OH, Report no. 443.

Harding, L.W. Jr., 1989, The use of aircraft and satellite remote sensing of phytoplankton chlorophyll concentrations in case2 estuarine waters of the Chesapeake Bay, Univ. of Maryland 1989 NASA-ASEE Summer Faculty Fellowship Program in Aeronautics and Research, 33.

Hatuch M.A. 1998, Modeling Expansion of Exotic Mussels on Lake Erie Sediments using Geographic Information Systems (GIS), a Master thesis, The Environmental Science Graduate Program, Dept. of Civil Engineering and Geodetic Sciences, The Ohio State University.

Herdendorf C. E. and D.M. Klarer 1998, The ecology of Old Woman Creek, Ohio: An Estuarine and Watershed Profile, a project report, the Old Woman Creek Research Center.

Hitoshi, T. and M. Suzuki 1982, Prediction of shoreline change and grain-size sorting at the Sendai bay coast, Sediment transport mechanisms in coastal environment and rivers, EUROMECH 310, pp.167-181.

Horstmann, O. and F. Molkenhuth 1996, Advanced Grid Modeling for Coastal and Nearshore Regions, The International Conference for Hydroinformatics, Zurich.

Ingham, A. E. 1992, Hydrography for Surveyors and Engineers, Blackwell Scientific Publication, London, 132 pp.

Jenson, S. K. and J. O. Domingue 1988, Extracting Topographic Structure from Digital Elevation Data for Geographic Information System Analysis, Photogrammetric Engineering and Remote Sensing, 54(11), pp. 1593-1600.

Kemp, K.K 1993, Environmental modeling with GIS: a strategy for dealing with spatial continuity, National Center for Geographic Information and Analysis, Santa Barbara, USA, Technical Report 93-3.

Kornus, W. and M. Lehner 1998, Photogrammetric point determination and DEM Generation Using MOMS-2P/PRIRODA three-line Imagery, International Archives of Photogrammetry and Remote Sensing, Stuttgart, Germany, 32(4), pp.321-328.

Lapine, L.A. 1991, Analytical Calibration of the Airborne Photogrammetric System Using A Priori Knowledge of the Exposure Station Obtained by Kinematic GPS Techniques, Report No. 411, Department of Geodetic Science and Surveying, The Ohio State University.

Li, R. 1997, Mobile Mapping An Emerging Technology for spatial Data Acquisition, *Photogrammetric Engineering and Remote Sensing*, 63(9), pp. 1165-1169.

Li, R. 1998, Potential of High-Resolution Satellite Imagery for National Mapping Products. *Photogrammetric Engineering and Remote Sensing*, 64(2), pp. 1165-1169.

Li, R. 1999, Coastal and Marine Geospatial Data for Decision Making, Digital Government Workshop, Columbus, Ohio, June14, 1999, 27pp.

Li, R. and G. Zhou 1998, Coastline Mapping and Change Detection Using One-Meter Resolution Satellite Imagery, A research project, Dept. of Civil Engineering and Geodetic Science, the Ohio State University.

Li, R. and G. Zhou 1999, Experimental Study on Ground Point Determination from High Resolution Airborne and Satellite Imagery, ASPRS Annual Conference, Portland, OR, May 17-21, pp.88-97.

Li, R., G. Zhou, A. Gonzalez, J. K. Liu, F. Ma, and Y. Felus 1998, Coastline Mapping and Change Detection Using One-Meter Resolution Satellite Imagery. Project Report submitted to Sea Grant/NOAA, 88 pp.

Li, R., G. Zhou, N.J. Schmidt, C. Fowler and G. Tuell 2001, Photogrammetric Processing of High-Resolution Airborne and Satellite Linear Array Stereo Images for Mapping Applications, *International Journal of Remote Sensing*, Accepted.

Li, R., G. Zhou, S. Yang, G. Tuell, N.J. Schmidt and C. Fowler 2000, A Study of the Potential Attainable Geometric Accuracy of IKONOS Satellite Imagery, Proceedings of 19th ISPRS Congress, Amsterdam, July 16-23, 2000 (CD-ROM).

Li, R., J.-K. Liu and Y. Felus 1999, Spatial Modeling and Analysis for Shoreline Change Detection and Coastal Erosion Monitoring. *Geoinformatics 99*, Ann Arbor, MI, June 19-21, pp.167-176.

Li, R., J.-K. Liu and Y. Felus 2001, Spatial Modeling and Analysis for Shoreline Change Detection and Coastal Erosion Monitoring, *Journal of Marine Geodesy*, 24(1), pp.1-12.

Liu, E. 1998, Developing Geographic Information System Applications in Analysis of Responses to Lake Erie Shoreline Change, MS. thesis, The Ohio State University.

Livingstone, D. E. and J.F. Raper 1994, Modeling environmental systems with GIS: theoretical barriers to progress. In *Innovations in GIS*, (ed. Worboys, M.), London, Taylor and Francis, pp. 229- 240.

Logan, T. 1989, The Ohio Agricultural Research and Development Center, The Ohio State University, Wooster Ohio, Phosphorus Analysis of Major Soil Series Samples from the Lake Erie Drainage Basin.

Madani, M. 1999, Real-Time Sensor-Independent Positioning by Rational Functions. *Proceeding of ISPRS Workshop on Direct Versus Indirect Methods of Sensor Orientation*, Barcelona, November 25-26, pp 64-75.

McCuen, H. 1998, *Hydrologic Analysis and Design*, Prentice Hall, Upper Saddle River, New Jersey.

Merchant, D. C. 1994, Airborne GPS-Photogrammetry for Transportation Systems, *Proceedings of ASPRS/ACSM*, pp. 392-395.

Neumaier, A. 1998, Solving III-conditional and Singular Linear System, A tutorial on Regularization, *SIAM Review*, 40(3), pp. 636-666.

NOAA 1997, Shoreline Mapping. <http://anchor.ncd.noaa.gov/psn/shoreline.html>.

OGC 1999, The OpenGIS™ Abstract Specification. Topic 7: The Earth Imagery Case, <http://www.opengis.org/public/abstract/99-107.pdf>.

Peuquet, D. J. and N. Duan 1995, an event-based spatio-temporal data model (ESTDM) for temporal analysis of geographical data, *International Journal of Geographical Information Systems*, 9(1), pp. 7-24.

Rapper, J. and D. Livingstone 1995, Development of a geomorphological spatial model using object-oriented design. *International Journal of Geographical Information Systems*, 9(4), pp. 359-384.

Rast, W. and G. F. Lee 1978, Summary Analysis of the north American Project(US portion) OECD Eutrophication Project, Nutrient Loading-Lake Response Relationships and Trophic State Indices, EPA-600/3-78-008.

Renard, K.G. and G.R Foster, G.A et al 1997, *Predicting Soil Erosion by Water: A guide to conservation planning with the Revised Universal Soil Loss Equation (RUSLE)*, Agricultural Handbook no. 703, UDA-SRS, Washington, D.C.

Schwab, D. and D. Sellers 1980, NOAA Data Report ERL GLERL-16, ftp://ftp.glerl.noaa.gov/publications/tech_reports/glerl-016/dr-016.html.

Schwab, D. J., J. R. Bennett, P. C. Liu, M. A. Donelan 1984, Application of a Simple Numerical Wave Prediction Model to Lake Erie *Journal of Geophysical Research*, 89(C3), pp. 3586-3592.

Shaw, B. and J.R. Allen 1995, Analysis of a Dynamic Shoreline at Sandy Hook, New Jersey Using a Geographic Information System, *Proceedings of ASPRS/ACSM*, pp.382-391.

Slama, C., C. Theurer and S.W. Henriksen 1980, Manual of Photogrammetry, American Society of Photogrammetry and Remote Sensing, Falls Church, Va.

Tao, C.V., and Y. Hu 2000, Investigation of the Rational Function Model. Proceeding of ASPRS Annual Convention, Washington D.C., May 22-26.

Tao, C.V., Y. Hu, J. B. Mercer, S. Schnick, and Y. Zhang 2000, Image Rectification Using a Generic Sensor Model - Rational Function Model, International Archives of Photogrammetry and Remote Sensing, 33(B3), pp. 874-881, Amsterdam.

The Great Lakes Forecasting System, the Department of Civil Engineering and Geodetic Science, The Ohio State University, <http://suoerior.eng.ohio-state.edu>.

US Department of Agriculture (USDA), ARS-Environmental Protection Agency, ORD 1975, Control of Water Pollution from Cropland,1(EPA-600/2-75-026A and ARS-H-5-1), Springfield, VA.

US Department of Agriculture (USDA), Wind Erosion Research Unit 1997, International Wind Erosion Symposium- Workshop Proceedings.

United States Geological Survey (USGS) 1990, On-line Open File Reports, Web site at [URL:http://geology.usgs.gov/open-file](http://geology.usgs.gov/open-file).

U.S Geological Survey (USGS) 1997, Report of Calibration of Aerial Mapping Camera, United States Department of the Interior.

Wang, Z. 1990, Principles of Photogrammetry (with Remote Sensing), Press of Wuhan Technical University of Surveying and Mapping and Publishing House of Surveying and Mapping, China.

Wewel, F. 1996, Determination of Conjugate Points of Stereoscopic Three Line Scanner Data of Mars'96 Mission, International Archives of Photogrammetry and Remote Sensing, Vienna, XXXI (B3), PP.936-939.

Whiteside, A. 1997, Recommended Standard Image Geometry Models. <http://www.opengis.org/ipt/9702tf/UniversalImage/TaskForc.ppt>.

Wischmeier, W. H. and D. D. Smith 1978, Predicting rainfall erosion losses- A guide to conservation planning, Agricultural Handbook no. 537, UDA-SEA, Washington, D.C.

Wolf, P. R. 1983, Elements of Photogrammetry. Second Edition. McGraw-Hill Publishing Company.

Worboys, M. F. 1992, A model for spatio-temporal information. Proceedings: the 5th International Symposium on Spatial Data Handling, 2, pp. 602-611.

Worboys, M. F. 1994. Unifying the spatial and temporal components of spatial information. Advances in GIS research (Proceedings, 6th International Symposium on Spatial Data Handling, Edinburgh, September 5-9, pp. 505-17.

Worthy, M. C., C. Herdendorf and K. Bedford et al 1983, Analysis of Great Lakes Seiche Affected Estuary Transport, A project report, Department of Civil Engineering and Geodetic Sciences, The Ohio State University.

Yang, X. 2000, Accuracy of Rational Function Approximation in Photogrammetry. Proceeding of ASPRS Annual Convention, Washington D.C., May 22-26.

Yen, C.C., K. Bedford, J. Kemp and R. Marshall 1990, a three-dimensional stereoscopic display and model control system for Great Lakes forecasts. IEEE Conference on Visualization, IEEE Press, pp. 194-201.

Zhou, G., and R. Li 2000, Accuracy Evaluation of Ground Points from IKONOS High-Resolution Satellite Imagery. *Photogrammetric Engineering and Remote Sensing*, 66(9), pp. 1103-1112.

4.2 Estimation of the shoreline soil-loss volume and contained phosphorus mass	41
4.3 Estimation of the contained phosphorus mass.....	46
4.4 Derivation of phosphorus concentration in the near-shore zone water	47
4.4.1 Coastal water-volume reflectance and chlorophyll derivation	48
4.4.2 Estimation of phosphorus concentrations in the near-shore zone	48
5. GIS-based modeling of surface transported contaminated sediment	51
5.1 Digital GIS-based modeling of the Old Woman Creek Area	51
5.2 Correlating the digitally-estimated and the measured runoff volumes.....	54
5.3 Modeling phosphorus intensity distribution in OWC coastal area	57
5.4 Soil loss modeling using the Revised Universal Soil Loss Equation (RUSLE)	60
5.5 Determination of the erosion-sedimentation relationship.....	61
5.6 Model consistency assessment	66
6. Conclusions	67
Acknowledgement	68
References	69